DOE/NE/32183--T2

Final Report on:
Department of Energy Grant
DE-FG01-94NE32183
(JHU No. C10.5065; APL Task FG363):

Nuclear Thermal Rocket Plume Interactions with Spacecraft

Principal Investigator:

Dr. Barry H. Mauk
The Johns Hopkins University
Applied Physics Laboratory
Laurel, Maryland 20723
301-953-6023
F: 301-953-6670
Barry_Mauk@jhuapl.edu

Co-Investigator:

Dr. Nikos A. Gatsonis
Mechanical Engineering Department
Worcester Polytechnic Institute
Worcester, MA 01609

Bd Final

DISCLAIMER

Nuclear Thermal Rocket Plume Interactions with Spacecraft

Summary of Accomplishments

This is the first study that has treated the Nuclear Thermal Rocket (NTR) effluent problem in its entirety, beginning with the reactor core, through the nozzle flow, to the plume backflow. The summary of major accomplishments is given below:

1. Determined the NTR effluents that include neutral, ionized and radioactive species, under typical NTR chamber conditions. Applied an NTR chamber chemistry model that includes conditions and used nozzle geometries and chamber conditions typical of NTR configurations.

2. Performed NTR nozzle flow simulations using a Navier-Stokes solver. We assumed frozen chemistry at the chamber conditions and used nozzle geometries and chamber conditions typical of NTR configurations.

3. Performed plume simulations using a Direct Simulation Monte Carlo (DSMC) code with chemistry. In order to account for radioactive trace species that may be important for contamination purposes we developed a multi-weighted DSMC methodology. The domain in our simulations included large regions downstream and upstream of the exit. Inputs were taken from the Navier-Stokes solutions.

4. Developed a hybrid DSMC and Particle-in-Cell (PIC) simulation methodology to model the transport of both neutral and charged species within the NTR plume, including plasma effects. Within the limited resources of this one year DOE grant, the full power of the hybrid DSMC-PIC methodology has not yet been applied to the combined neutral/ionized component backflow problem. Only specialized cases have been run to date.

5. This project resulted in a Masters of Science Degree Thesis ("Nuclear Thermal Rocket Effluent Assessment and Direct Simulation Monte Carlo of Plume Backflow", Jared Busby, May, 1996, Worcester

Polytechnic Institute - WPI). In addition, two undergraduate students completed their senior thesis projects on NTR related issues ("Nuclear Thermal Rocket Effluent and Performance Study", Richard Nanson and Sarah MacIlihenny, April, 1996).

6. A detailed report follows this summary. Major results were reported at the 31st AIAA Thermophysics Conference (AIAA 96-1850; June 17-20, 1996/New Orleans, LA). A reprint of our paper is attached to our detailed report.

7. Since the completion of this project, work on hybrid (DSMC-PIC) methodologies have continued by Prof. Gatsonis' group at WPI. With these enhance capabilities the NTR plume could be further investigated by:

1. Including a chemically reacting Navier-Stokes code for the nozzle flow evaluation.
2. Applying the full capabilities of the developed DSMC-PIC code in the plume in order to address fully the potential for backflow due to the neutral and ionized plume component.

Final Report

APL Subcontract No. 710512

NUCLEAR THERMAL ROCKET PLUME INTERACTIONS WITH SPACECRAFT

Dr. Nikos A. Gatsonis
Assistant Professor

Jared Buzby
Graduate Assistant

Xuemin Yin
Graduate Assistant

Mechanical Engineering Department
Worcester Polytechnic Institute
Worcester, MA 01609

Submitted to:
Johns Hopkins University Applied Physics Laboratory
Dr. Barry Mauk, Technical Contract Representative
Johns Hopkins Rd.
Laurel, MD 20723

Abstract

Nuclear Thermal Rocket (NTR) effluents include neutral and ionized hydrogen propellant, traces of reactor fuel material, including radioactive material and fission products. Backflow of these effluents presents a contamination risk to the spacecraft. The neutral, ionic and non-propellant composition of an NTR plume can vary significantly depending on design and operating conditions. This complicates the analysis especially in cases of partially ionized plumes because modeling must combine techniques that have been utilized for both purely neutral and plasma plumes. This study addresses some of the issues associated with NTR effluxes and plume backflow modeling.

The effluent composition of an NTR plume is investigated. The nozzle flow is modeled with an axisymmetric Navier-Stokes code using a typical NTR nozzle geometry and characteristic chamber conditions. The species composition at the nozzle exit is based on the assumption of frozen chemistry to the chamber conditions. High temperature and radiation induces ionization and dissociation of the propellant in the chamber. Results of a chemistry model are presented for typical NTR chamber conditions. The reactor material is also included in the efflux using a model based on the reactor power and the reactor mass loss rate. Species found at the nozzle exit include H_2, H, H_2^+, H^+ and traces of reactor core materials, ZrC, $U_{0.1}Zr_{0.9}C$ and UC.

In order to model the transport of neutrals and charged species found in the NTR plume the required modifications to the Direct Simulation Monte Carlo (DSMC) and Particle-in-Cell (PIC) methodologies are presented. A DSMC-PIC based code is developed and includes two dimensional axisymmetric geometry, general inflow boundary conditions, and variable particle weights for the plume components. The code uses a primary grid for neutral transport and a secondary grid for the estimation of electric fields and ion motion. The version of the code used in this study does not include the self-consistent electric fields into the ion motion.

The plume simulations begin near the nozzle exit using as inputs the Navier-Stokes flow profiles. Plume species include H_2, H, H_2^+, H^+ and reactor core materials, ZrC, $U_{0.1}Zr_{0.9}C$ and UC. Simulations correspond to chamber temperatures of 2,700 K and chamber pressures of 10 and 100 kPa. The backflow characteristics and species separation confirm previous findings. The backflow is shown to mainly composed of the light neutral and ion propellant species while heavy reactor species are confined in the downstream area of the thruster exit. The flow field characteristics, the effects of the boundary layer, and species separation are discussed. Due to the large ionized component of the plume, plasma effects may modify the backflow fluxes.

Table of Contents

Nomenclature

Symbol	Definition
A	area
A^*	the area of a nozzle throat
A_e	the area of an exit
A_e/A^*	an area ratio
d_p	molecular diameter
D_e	diameter at nozzle exit
$[e]$	concentration of species e
E_f	energy production of fast-ion producing species
W_p	ratio of real to computational particles for species p
F_i	degree of separation of species i
[H]	concentration of species H
$[H_2]$	concentration of species H_2
$[H^+]$	concentration of species H^+
$[H_2^+]$	concentration of species H_2^+
Isp	The specific impulse
k_i	reaction rate for ith reaction
k_B	Boltzman's constant
Kn	Knudsen number
Ln	nozzle length
L	a characteristic dimension
m_i	mass of particle i
$\dot{m}$	mass flux
n	number density
n_f	particle density of the fast-ion producing species
N	total number of particles
N_A	Avogadro's number
P	pressure
P_a	ambient pressure
P_c	chamber pressure
P_W	power
P	probability of collision
$\dot{Q}_r$	energy deposition rate per unit volume

R	gas constant
R_u	universal gas constant
T	temperature
T_c	chamber temperature
T_{ref}	reference temperature
T	thrust
V_C	cell volume
α	degree of dissociation
γ	ratio of specific heats
γ_i	probability of the energy absorption
ε_n	area ratio
λ	mean free path
σ_{th}	thermal neutron cross section
σ_T	collision cross section

1. Introduction

One of the primary candidates for nuclear space power and propulsion is the Solid Core Nuclear Thermal Rocket (NTR). Many different concepts have been proposed to date for a variety of missions [*Corban*, 1993; *Borowski et al.*, 1994]. The general operating principle of a NTR is based on the heating of hydrogen to a high temperature followed by the expansion through a conventional convergent-divergent nozzle. The result is a high speed hydrogen plume that may contain other constituents that are of concern to the successful operation of the spacecraft.

The most distinct group of plume effluents is the propellant, most likely atomic and molecular hydrogen. The second group of effluents contains ionized material due to radiation or other chemical interactions. The most important group for contamination purposes contains radioactive reactor and fission materials. These are products of the high temperature interactions between hydrogen gas and the solid fuel element constituents. Also, fission products such as Sr, I, Xe, and Nd contribute to this group since complete containment is probably impossible due to the extremely high temperatures of the fuel elements [*Bokor*, 1991]. From the limited test experience from the NERVA and Rover programs, some estimates exist in regard to the reactor material loss. However, the mechanisms that cause the erosion of fuel particles are not currently well understood [*Pelaccio*, 1994; *Bokor*, 1991]. The presence of radioactive particles in the plume could serve to further dissociate, and ionize the neutral plume constituents. Finally, it is expected that non-propellant material sputtered from the chamber or thruster components exist in the plume. A portion of these neutrals will further undergo chemical reactions in the nozzle and plume.

One is concerned with the extent to which these constituents backflow towards the spacecraft since they can lead to contamination, surface deposition, surface damage due to chemical and/or sputtering effects, optical emissions that can affect optical devices such as star cameras, and communications problems due to the ionized constituents. Thus, it is important to understand the backflow properties of thruster plumes. These issues are discussed at length by *Mauk et al.* (1993) in the context of Nuclear Electric Propulsion technologies. The general concepts discussed there hold true for NTR technologies as well. From the proposed NTR designs, operational parameters often span two orders of magnitudes in pressure or thrust levels [*Clark*, 1991]. In addition, the degree of ionization critically depends on the level of radiation and the overall chemical interactions. Subsequently, the neutral, ionic and non-propellant composition of an NTR plume can vary significantly depending on design and operating conditions. This

complicates the analysis especially in cases of partially ionized plumes because modeling must combine techniques that have been utilized for both purely neutral and plasma plumes. This study addresses some of the issues associated with NTR effluxes and plume backflow modeling.

1.1 Technical Background and Review

A large number of studies have been devoted to the analysis of neutral plume backflow from chemical rockets. The analysis is carried out for high pressure plumes with the method of characteristics or Navier-Stokes solvers [*Smith*, 1991]. The so-called "nozzle-lip effect" has been found to be very important to the backflow phenomena of interest in the present work [*Hueser et al.*, 1986; *Campbell*, 1989]. In addition, early on in the investigation of rarefied flows it was pointed out by *Bird* [1988] that thermal and pressure diffusion effects are very important, especially as the flow becomes more rarefied. *Boyd et al.*, [1991] compared DSMC, Navier-Stokes and experimental investigations of small nitrogen thrusters. These comparisons showed that as in the case of shock waves, Navier-Stokes failed to predict the expanding flow. *Chung et al.* [1993] compared Navier-Stokes and DSMC solutions, to experimental data for low-density nozzle flows. The major finding was that DSMC compares favorably with the data both in the densities and rotational temperatures of the gas. The interactions of the plume with the free-stream regions is also of importance for NTR backflow. The penetration of the background gases into the expanding gas changes significantly the general structure of the interaction [*Mc Ginnis et al.*, 1973]. DSMC comparisons with experimental data by *Campbell* [1991] verified that at high altitudes the plume-free stream flowfield is in a non-equilibrium state. In addition the chemical interactions of the plume gases with the free-stream will depend on the neutral, ionic and electromagnetic characteristics of the background. This is particularly important since NTRs are proposed for missions that encompass a variety of ambient environments. The first application of DSMC for the study of a plume from a nuclear rocket appeared in *Chung et al.* [1992; 1993]. It was shown that the flow is primarily determined by the thin subsonic layer at the nozzle lip and that the backflow consists of mostly lighter species due to the separation. *Chung et al.* however used a very simple plume composition model.

Another complexity of NTR plumes is their potentially significant ionized component. The resulting plasma environment requires modeling approaches that are fundamentally different from those used in the analysis of neutral plumes described above. Plasma plumes have received considerable less attention than their neutral counterparts. A recently developed Particle-In-Cell based model by *Roy et al.* was applied to ion thruster plumes [1996 a,b and references therein]. It was shown that plume electric fields transport ions in the backflow region and generate a low

energy plasma cloud about the spacecraft. Plasma effects can also be manifested with the formation of large-scale (kilometer size) plasma clouds. *Gatsonis and Hastings* [1991] developed a three-dimensional model in order to address the plasma cloud evolution and the induced environment following a neutral release from an orbiting spacecraft.

1.2 Modeling Approach

It is clear that there is need for fundamental understanding of contamination and other induced environment effects from an NTR. Our approach is to study the NTR effluents and begin the development of a model which will allow the simulation of transport of neutrals and ions in an NTR plume. The effluent problem is treated in this study in a unified way beginning with conditions at the reactor core and nozzle chamber through the nozzle flow to the plume backflow as shown in Figure 1.1.

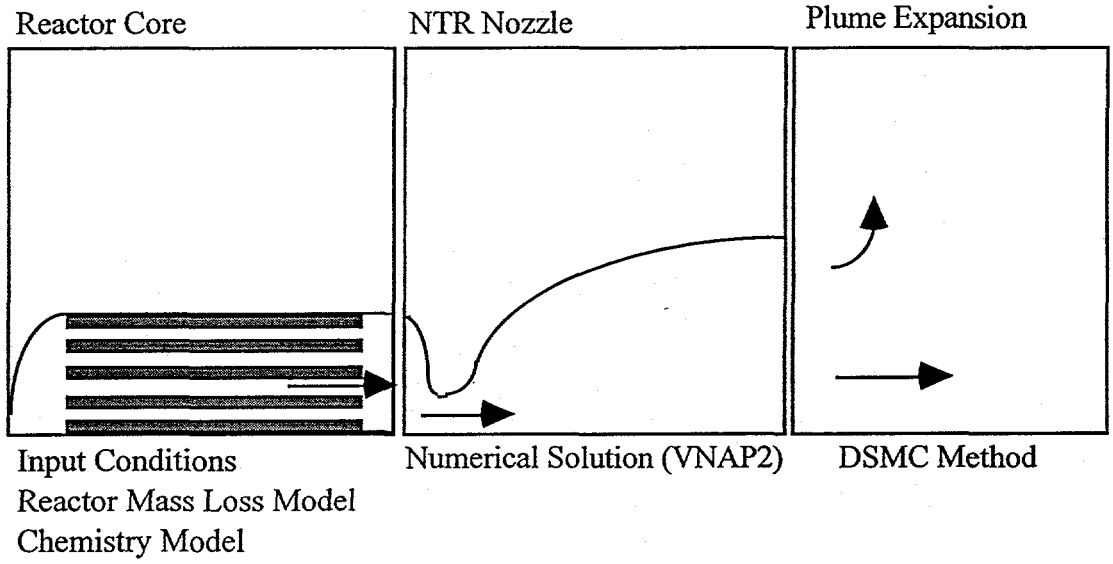

Figure 1.1 Schematic of NTR plume modeling approach.

Specifically, the following aspects are addressed in the present work:

- Nozzle Flow and Effluent Evaluation
  The nozzle flow is evaluated using the Navier Stokes solver VNAP2 [*Cline*, 1981]. The flow is based on chamber pressure and temperature typical of NTR configurations. The nozzle

geometry is taken with an area ratio of 200 and an exit diameter of 2 m. Dissociation and ionization in the NTR chamber are accounted for with a chemistry model that includes high temperature and radiation effects. The effluent composition at the nozzle exit is assumed to be frozen to the chamber conditions and is determined using the local flow parameters. The nozzle exit flow includes propellant species H, H_2, H^+ and H_2^+ and reactor material ZrC, $U_{0.1}Zr_{0.9}C$, and UC. The reactor flux is estimated assuming a loss rate of 0.2 g/minute/per fuel element.

- Plume Backflow and the DSMC-PIC Methodology:
  An axisymmetric code based on DSMC and Particle-in-Cell (PIC) methodologies with chemistry is developed for this study. Inputs to the code are taken from the nozzle flow Navier-Stokes solutions. The simulations begin close to the exit of the NTR nozzle and include the boundary layer profile and the species composition as established by the chamber conditions. Due to the large variation in species concentration (up to 7 orders) and molecular mass (light hydrogen propellant and heavy reactor materials), the code assigns species to separate groups with different numbers of real particles per computational particle (particle weights, W_p). This allows for accurate collision rate determination and consequently backflow estimation. The code includes a PIC based methodology for the treatment of ion species but currently does not account for self-consistent electric fields.

A review of operating parameters of solid core NTRs is presented in Section 2. The nozzle flow modeling approach and results are presented in Section 3. The chamber chemistry model, the neutral and ion propellant composition are presented in Section 4.1. The reactor mass loss model and results are presented in Section 4.2. The DSMC-PIC methodology and preliminary results from NTR plume simulations are discussed in Section 5.

2. Solid Core Nuclear Thermal Rockets

This work focuses on solid core nuclear thermal rocket plumes. This choice is due to the high specific impulses of approximately 850 seconds already achieved in the NERVA program [*Corban*, 1993]. Furthermore, solid core NTRs are a near term technology due to testing experience and recent developments in the area of material processing. As we discussed in the introduction in a solid core NTR low temperature (approximately 200 K) hydrogen at high pressures is passed through the nuclear reactor core [*Peery et al.*, 1993]. After heating, the hydrogen propellant is fed into a chamber and then expands through a converging-diverging nozzle. Most of the NTR concepts have been derived from the NERVA and Rover programs. Between the years 1955 and 1972 these programs produced twenty reactor tests at full power and temperature operating conditions. These reactor tests are the only ones performed in the United States and have formed the background of NTR technology. Further design improvements are now possible due to new material coatings which may operate at higher temperatures [*Bokor et al.*, 1991; *Pelaccio et al.*, 1991].

A typical NERVA-derived concept shown in Figure 2.1 uses a graphite composite hexagonal fuel element with circular axial propellant channels. All fuel element surfaces are coated to protect the fuel from corrosion by hot hydrogen. Fuel elements may be clustered to provide variable thrust levels. Operating temperatures as high as 2,500 K have been demonstrated in NERVA tests with a corresponding specific impulse of 850 seconds. Future developments aim to achieve specific impulses as high as 900 seconds [*Corban*, 1993].

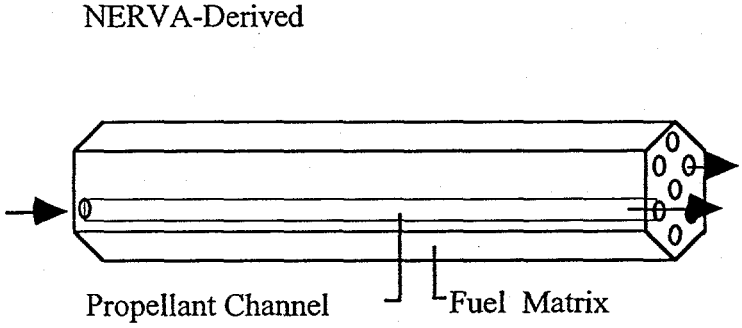

Figure 2.1 Schematic of a NERVA derived NTR design.

The Particle Bed Reactor (PBR) shown in Figure 2.2 is unique in its use of small (400-500 μm diameter) coated spherical fuel elements. These fuel elements are packed between two concentric porous cylinders. The propellant passes radially from the outer cylinder, "cold frit", through the fuel particles and is heated directly, passing through the inner cylinder, "hot frit", and exhausted to the rocket chamber. A number of these fuel elements may be used to produce variable thrust levels. Conceptual design studies are currently underway aiming at chamber temperatures of 2,770 K and specific impulses of 915 seconds [*Corban*, 1993].

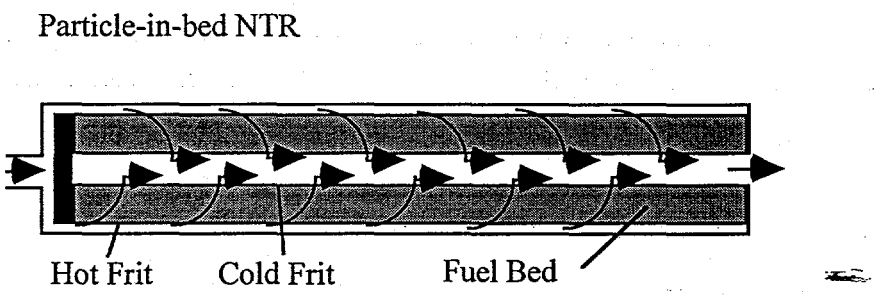

Figure 2.2. Schematic of a Particle-in-bed NTR.

A similar to the NERVA NTR program began in 1959 in the former Soviet Union (CIS) and continued until 1988 with considerable advances. This program included extensive nuclear and non-nuclear subsystem tests, including fuel element and reactor tests. However, this program concluded in 1988 without the completion of system level tests [*Corban*, 1993]. The "Twisted Ribbon" design of the CIS shown in Figure 2.3 is quite similar to the NERVA concepts, except that the propellant channels spiral, offering greater surface area for a given length. The maximum fuel element operating temperature is expected to be about 3,200 K. Reactor tests have produced chamber temperatures of 3,100 K for one hour. This concept extends the envelope of NTR operating temperatures to a great extent. Currently conceptual studies are underway to verify CIS results [*Corban*, 1993].

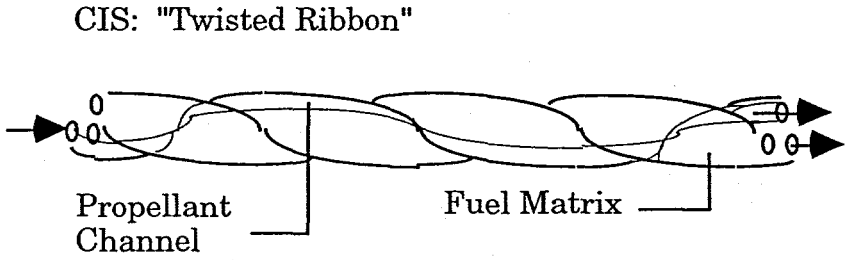

Figure 2.3 Twisted Ribbon NTR schematic.

2.1 NTR Operating Parameters

The fundamental difference between the three NTR's discussed above is the design of the reactor core itself. It is within the reactor core that the neutral and ion contaminants, such as radioactive particles, enter the flow. The reactor core also defines the state of the gas in the chamber before it enters the nozzle. Therefore a fundamental understanding of the reactor core and its operating conditions is critical to any contamination study involving NTR technologies. In addition any parametric investigation and numerical contamination study must consider operating parameters consistent with current and proposed designs. These parameters include the chamber pressure P_c, chamber temperature T_c , the nozzle exit diameter D_e, the area ratio A_e/A^* and the mass flow rate $\dot{m}$.

Chamber temperature is an important parameter used in NTR performance optimization. In order to increase the I_{sp} the T_c is increased to a limit determined by the melting point of the materials in the reactor core and nozzle chamber. The NERVA tests achieved chamber temperatures of 2,500 K while the CIS design achieved temperatures of 3,200 K, close the melting point of materials [*Corban*, 1993; *Pelaccio et al.*, 1994].

Operating chamber pressures, P_c, in the numerous solid core NTRs studies range from 3.45 to 6.9 MPa [*Clark et al.*, 1992; *Corban*, 1993; *El-Genk et al.*, 1993; *Johnson et al.*, 1993; *Lee*, 1993; *Pelaccio et al.*, 1991; *Scheil et al.*, 1993;*Wetzel et al.*, 1993; *Zweig et al.*, 1993]. Low pressure NTR concepts have also been considered [*Ramasthaler et al.*, 1990] and several nozzle optimization studies considered pressures as low as 10 kPa (*Stubbs et al.*, 1991; 1993; *Davidian and Kacynski.*, 1991; *Watanabe*, 1992].

Area ratios A_e/A^* used in various NTR studies range between 100 and 500 with exit diameters between 2.5 and 7 meters [*Stubbs et al.*, 1991; *Clark et al.*, 1992]. Table 2.1 summarizes basic operating parameters used in previous NTR studies. It should be noted that nozzle optimization is an important area of ongoing research.

Reference	D_e (m)	A_e/A^*	P_c (MPa)	T_c (K)	$\dot{m}$ (kg/s)
Chung et al., 1992	2.27e-3		Pe= 0.001	Te= 1000	3.04e-6
Chung et al., 1993	2.8 (0.1)	100	0.1	2700, 3200, 3600	
Clark et al., 1992	4.16	500	6.9	2200-3300 (2500, 2700)	37
Corban, 1993	2.44	200	5.4	3000	
Culver et al., 1994		300	14	2556	11.8
Davidian et al., 1991	1.65,1.8, 2.3, 5		0.069, 0.21, 0.69, 2.1, 6.9,21	2700, 2900, 3100	
El-Genk et al., 1993			1-5	2900	24-32
Johnson et al., 1993		200	6.9	2700	
Lee, 1993			3.9	2300	35.6
Leyse et al.,	.691, 2.18	100	0.34, 34	2500, 3200	2.09,2.20 2.61,2.64
Pelaccio et al., 1991	4.15	100, 200, 500	1.4, 3.1, 3.4, 6.9	2200-3300 (2500, 2700, 3100)	20-300 (37)
Scheil et al., 1993	3.76	200	3.4	3600	38.7
Stubbs et al., 1991	5.6	100	0.001-10.1	3600	
Stubbs et al., 1993	2.8	100	0.01, 0.1, 1	2700, 3200, 3600	
Watanabe, 1992			0.01, 0.1, 1.0, 10	2000-4000	
Wetzel et al., 1993		100, 150, 200, 240, 300, 500	0.14-6.9	2700-3300	
Zweig et al., 1993		200, 300, 500, 700	3.4-14 (5.4)	2450	25.2

Table 2.1 Nuclear Thermal Rocket studies and parameters utilized.

3. NTR Nozzle Flow Modeling

The NTR nozzle flow is modeled using VNAP2, an axisymmetric code for the compressible Navier-Stokes equations [*Cline*, 1981]. The code is based on the Mac Cormack finite difference formulation and includes a turbulent model. Figure 3.1 shows the physical and computational spaces used by VNAP2.

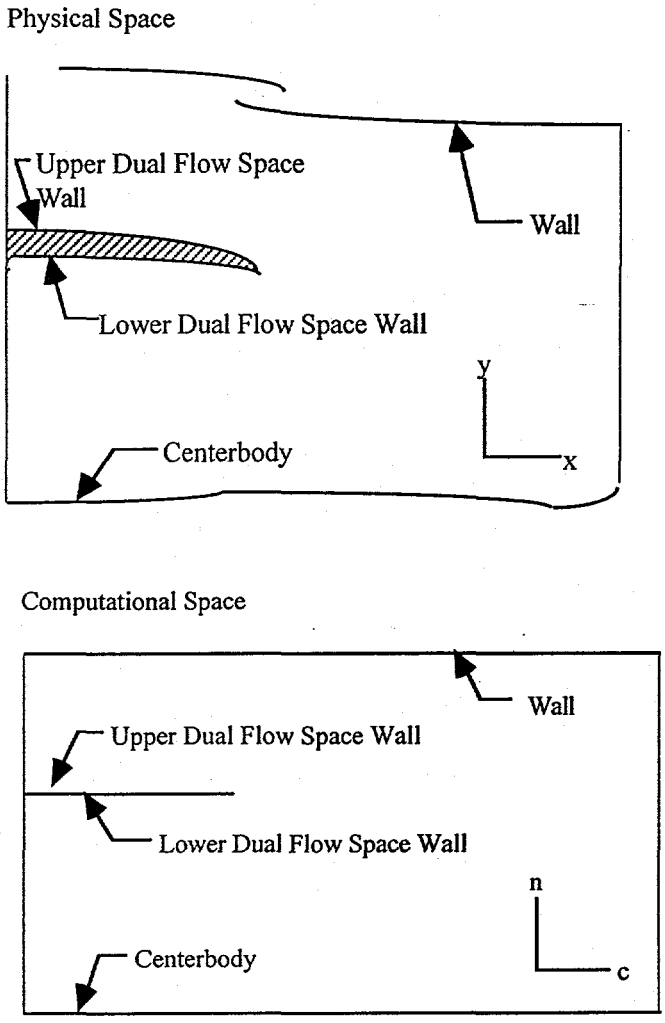

Figure 3.1 Physical and Computational Spaces used by VNAP2 (adapted by Cline, 1981)

The upper boundary, or *wall*, may be a solid boundary, a free-jet boundary, or an arbitrary subsonic (normal to the boundary) inflow/outflow boundary. The lower boundary, or

centerbody, may be a solid boundary or a plane (line) of symmetry. The wall and centerbody may be arbitrary curved boundaries provided the y coordinate is a single value function of x. The left boundary is a subsonic, supersonic, or mixed inflow boundary, whereas the right boundary is a subsonic, supersonic, or mixed outflow boundary or a subsonic inflow/outflow boundary [*Cline*, 1981].

Input parameters required for the nozzle VNAP2 calculations are the chamber stagnation values and nozzle geometry. In an NTR the flowfield at the nozzle entrance is defined by the reactor core. The study of the flow within the reactor core is beyond the scope of this work as it depends on the very details of the reactor design [*Storms et al.*, 1991]. To simplify the analysis, our nozzle flow calculations are based on chamber conditions typical of NTR configurations.

Based on the review presented earlier, chamber pressures considered in our study are varied between 10 kPa and 1 MPa and chamber temperatures between 2500 K and 2900 K. The nozzle contour shown in Figure 3.2 is a parabola fitted to connect a tangent point on the downstream throat circle and a specific exit coordinate [*Davidian and Kacynski,* 1991].

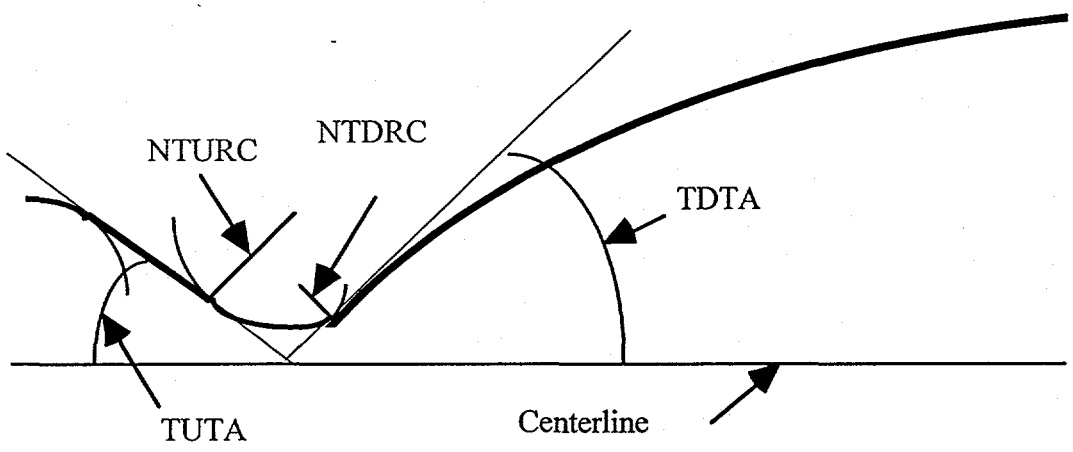

Figure 3.2. Baseline Geometric Definition and Parameters.

The parameters needed for the definition of the nozzle are the nondimensional throat upstream radius of curvature (NTURC), nondimensional throat downstream radius of curvature (NTDRC), throat upstream tangent angle (TUTA), and the throat downstream tangent angle (TDTA). The nozzle length L_n is taken to be 80% of a 15° cone nozzle with the same throat radius, downstream radius of curvature and area ratio. The length is calculated from the following equation [*Huzel et al.*, 1967],

$$L_n = 0.8\frac{r_t\left(\sqrt{\varepsilon_n}-1\right)+RWTD\left(\sec a_n-1\right)}{\tan a_n} \tag{3.1}$$

where r_t is the throat radius, ε_n is the area ratio, *RWTD* is the downstream throat radius of curvature, and α_n is the cone half angle. The parameters that define the nozzle are shown in Table 3.1 and have been adapted from *Davidian and Kacynski* [1991] but with an exit diameter of D_e=2 meters and an area ratio A_e/A^*=200. This choice of parameters results in a nozzle length of L_n=3 m.

Chamber Contraction Ratio	5.00
NTURC	2.0623
NTDRC	0.19
TUTA	26.25°
TDTA	32.0°
L_n	80% of a 15° Cone

Table 3.1 Nozzle Geometric Parameters.

The Mach number contours of a sample VNAP2 calculation are shown in Figure 3.3. Case 1 corresponds to P_c=10 kPa and T_c=2,700 K. The flow is shown to accelerate from the chamber to M=1 at the throat and reach the exit plane with M=8.09. Figure 3.3 demonstrates the development of a boundary layer along the nozzle wall as the flow expands from the throat to the exit plane. As we discuss later, the boundary layer plays a crucial role in the backflow.

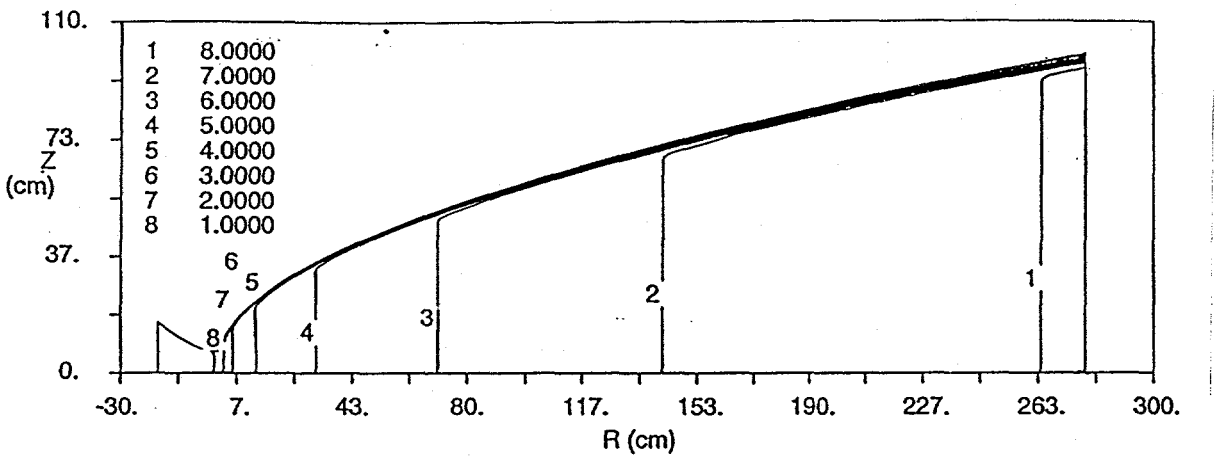

Figure 3.3. Mach Number Profiles from VNAP2 (Case 1: P_c=10 kPa, T_c=2,700

4. NTR Effluent Evaluation

4.1 Neutral and Ionized Propellant Effluents

The hydrogen propellant in the chamber and nozzle of an NTR subjected to high temperature and radiation undergoes dissociation and ionization. Chemical reactions depend upon many local flow and nozzle geometry details [*Stubbs et al.*, 1991]. As an approximation, it is assumed in the present study that the chemical composition is defined by chamber conditions and remains frozen up to the nozzle exit. Following *Watanabe* [1991] we assume that five species (H, H_2, H^+,H_2^+, and electrons) are present in the chamber. For these species, the following chemical reactions are considered:

$$H_2 + X \rightarrow H_2^+ + e + X \quad (4.1)$$

$$H_2 + X \rightarrow H + H + X \quad (4.2)$$

$$H + X \rightarrow H^+ + e + X \quad (4.3)$$

$$H_2 + M \rightarrow H + H + M \quad (4.4)$$

$$H + H + M \rightarrow H_2 + M \quad (4.5)$$

$$H_2 + e \rightarrow H + H + e \quad (4.6)$$

$$H^+ + e + e \rightarrow H + e \quad (4.7)$$

$$H_2^+ + e \rightarrow H + H \quad (4.8)$$

In the first three reactions (4.1-4.3), X represents gammas, neutrons and fission products. Among those gammas do not ionize effectively the hydrogen. However, the fission products that are released into the chamber are not stable isotopes and can fission furthermore releasing ions, neutrons and gammas. These secondary ions interact very effectively with the hydrogen. The radiation reaction rate k_r (r=1,2,3) is given by

$$k_r = G_r \gamma_i \dot{Q}_r \quad (4.9)$$

where G_r is the number per 100 eV of absorbed radiation, γ_i is the absorption probability and $\dot{Q}_r$ is the energy deposition rate per unit volume (Wm^{-3}). The G-values are given for each reaction by G_1=2.75x10^{-2}eV^{-1}, G_2=3.03x10^{-2} and G_3=4.33x10^{-2} eV^{-1}. The absorption probability in a gaseous mixture with concentrations n_i and n_j is defined as $\gamma_i = n_i/(n_i + \alpha_{ij} n_j)$, where α_{ij} is the ratio of the effective atomic masses of species i and j. Finally, the deposition rate is given by

$$\dot{Q}_r = E_f n_f \sigma_{th} \phi_{th} \quad (4.10)$$

where, n_f, is the density of the fission products, E_f is the energy released per fission, ϕ_{th} is the thermal neutron flux and σ_{th} is the cross section. Hydrogen dissociation is expressed by reactions (4.4) and (4.6), recombination by reaction (4.5), and electron recombination by reactions (4.7) and (4.8). The reaction rates are given by *Watanabe*:

$$k_4 = 6.34\times10^{-34}\left(\frac{T}{2870}\right)^{-1.2} \text{ cm}^6\text{s}^{-1} \tag{4.11}$$

$$k_5 = 3.15\times10^{-10}\exp\left(\frac{-95500}{RT}\right)\text{cm}^3\text{s}^{-1} \tag{4.12}$$

$$k_6 = 3.17\times10^{-13}\exp\left(\frac{-203}{RT}\right)\text{cm}^3\text{s}^{-1} \tag{4.13}$$

$$k_7 = 8.7\times10^{-20}\left(\frac{T}{298}\right)^{-4.5} \text{ cm}^3\text{s}^{-1} \tag{4.14}$$

$$k_8 = 1.6\times10^{-8}\left(\frac{T}{300}\right)^{-0.43} \text{ cm}^3\text{s}^{-1} \tag{4.15}$$

In steady state the rate equations of reactions (4.1-4.8), supplemented by the species conservation equation, the charge neutrality equation and the ideal gas law, result in a system that provides the concentration of H, H_2, H^+, H_2^+ and electrons in the NTR chamber.

The above model has been applied for chamber conditions as shown in Table 4.1 and radiation absorption rates of $\dot{Q}_1=10^5$, $\dot{Q}_2=10^6$ and $\dot{Q}_3=10^7$ Wm^{-3} respectively. For ^{235}U, which is a common fuel source for NTRs, E_f=168 MeV, σ_{th}=590x10^{-28} m^2 and ϕ_{th}=10^{20} m^{-2}s^{-1} [*Watanabe*, 1992]. These deposition rates correspond to n_f= 10^{12}, 10^{13}, 10^{14} m^{-3} fuel densities respectively. Table 4.1 shows also the total chamber number density n_c.

P_c (kPa)	T_c (K)	n_c(m^{-3})
10	2700	2.683x10^{23}
100	2700	2.683x10^{24}
1000	2700	2.683x10^{25}
10	2900	2.498x10^{23}
100	2900	2.498x10^{24}
1000	2900	2.498x10^{25}

Table 4.1. Number density for various NTR chamber pressure and temperatures.

Figure 4.1 shows the atomic hydrogen fraction $X(H)=[H]/n_c$ which for $n_c \sim [H]+[H_2]$ becomes identical with the degree of dissociation. The number fraction $X(H)$ is shown to decrease with increasing pressure. Higher temperatures increase the hydrogen fraction but the effects are more pronoun at lower chamber pressures. Also, for a given chamber P_c and T_c larger values of radiation deposition $\dot{Q}_r$ result in an increase in $X(H)$ especially at lower pressures.

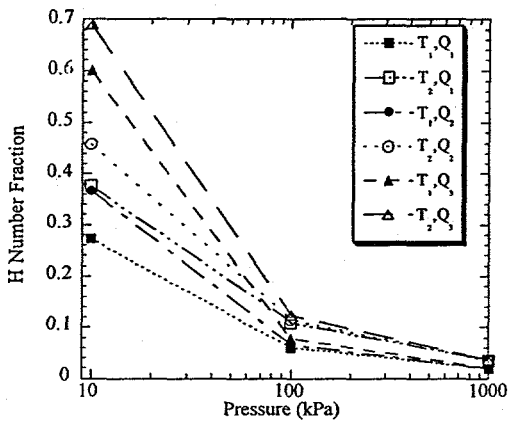

Figure 4.1. Number fraction $X(H)$ in an NTR chamber (T_1=2700 K, T_2=2900 K, $\dot{Q}_1=10^5$, $\dot{Q}_2=10^6$, $\dot{Q}_3=10^6$ Wm^{-3}).

Figures 4.2 and 4.3 show the ionized species fraction $X(H_2^+)=[H_2^+]/n_c$ and $X(H^+)=[H^+]/n_c$ respectively. Although the fractions are very small the resulting number densities of the ionized propellant are large enough for plasma effects to become important. For example, at a chamber pressure of 1000 kPa and temperature of 2700 K the number densities become $[H^+]\sim 10^{19}$ m^{-3} and $[H_2^+]\sim 10^{18}$ m^{-3}. Figures 4.2 and 4.3 demonstrate also that for given chamber conditions the ionization fraction increases with increasing radiation deposition rate. Higher pressures result in reduced ionization fractions while temperature variation shows to have minimal effects.

It should be noted here that a complete determination of the radiation absorption process requires detailed knowledge of the reactor fluxes and chamber/nozzle flow conditions well beyond the scope of this study. Therefore, these results are to be taken as indicative of the trends to be expected in an NTR chamber. Given the importance of the radiation induced ionization as well as other ionization reactions it is necessary for more detailed chemistry models to be included in future studies.

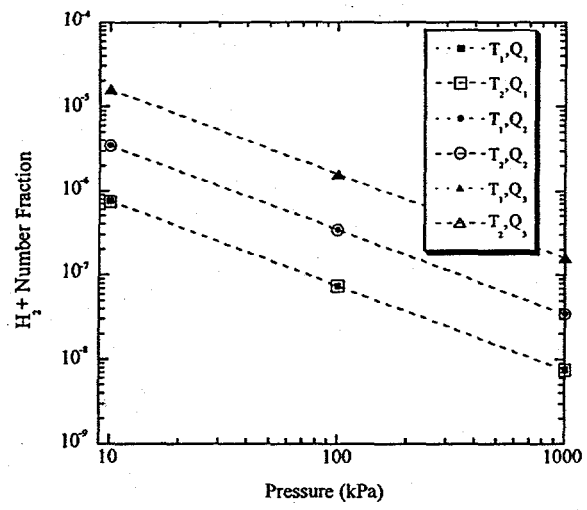

Figure 4.2. Number fraction $X(H_2^+)$ in an NTR chamber (T_1=2700 K, T_2=2900 K, $\dot{Q}_1$=10^5, $\dot{Q}_2$=10^6, $\dot{Q}_3$=10^6 Wm^{-3}).

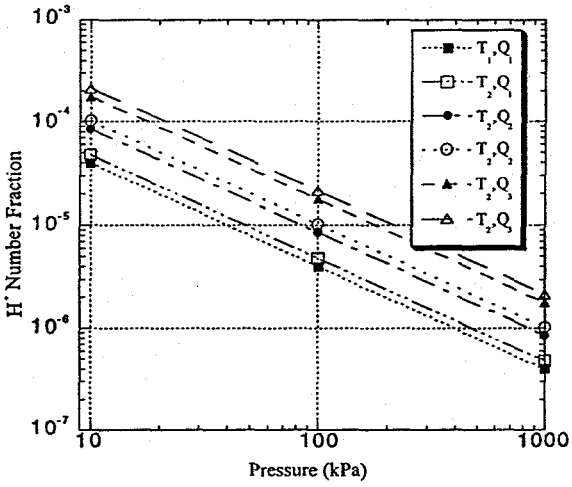

Figure 4.3. Number fraction X(H^+) in an NTR chamber (T_1=2700 K, T_2=2900 K, $\dot{Q}_1$=10^5, $\dot{Q}_2$=10^6, $\dot{Q}_3$=10^6 Wm^{-3}).

4.2 Non-propellant (Reactor Core) Effluents

The complete determination of non-propellant effluents in the nozzle and plume of an NTR is very difficult. This efflux is primarily the result of the corrosive effects of high temperature hydrogen on the reactor materials. The non-propellant efflux includes fuel material, fuel matrix and coatings materials and other compounds. In addition fission products and byproducts are part of the efflux. The phenomena that contribute to corrosion of the reactor fuel elements and structure are not completely understood. Experimental results are also limited and based on the Rover/NERVA tests. Tests of the Pewee reactor demonstrated that during relatively short operation times the reactor lost mass at a rate of 0.2 g/minute per fuel element [*Pelaccio et al.*, 1994]. The mass loss rate was found to increase with the time of operation of the reactor. Also, the number of reactor cycles was found to greatly increase the crack size of the fuel elements. It is therefore expected that longer operation will result in materials other than the coating to be eroded by hydrogen. An extensive review of the subject is given by *Bokor et al.* [1991] and *Pelaccio et al.* [1994; 1995].

A simple model is used to quantify the material loss rate in this study. It is assumed that the reactor material lost consists of 25% ZrC coating, 50% $U_{0.1}Zr_{0.9}C$ matrix and 25% UC fuel particles. This composition is based upon the assumption that the reactor operates for times long enough for materials other than the coatings to be eroded. The reactor mass loss rate is taken as 3.33×10^{-6} kg/s/fuel element and corresponds to a Pewee type reactor operating at a power density of 1.2 MW per fuel element. Given the mass flow rate $\dot{m}$ as obtained from VNAP2, the reactor power P_W, the number of fuel elements and the total mass flow rate of reactor material can be evaluated. Results of the above procedure are shown in Table 4.2 for the pressure range of 10-1,000 kPa and temperature range of 2,700 and 2,900 K.

	P_c	T_c	$\dot{m}$ (kg/s)			
	(kPa)	(K)	Propellant	ZrC	$U_{0.1}Zr_{0.9}C$	UC
1	10	2700	3.128×10^{-2}	8.259×10^{-7}	1.651×10^{-6}	8.259×10^{-7}
2	100	2700	3.161×10^{-1}	8.505×10^{-6}	1.701×10^{-5}	8.505×10^{-6}
3	1000	2700	3.003	8.526×10^{-5}	1.705×10^{-4}	8.526×10^{-5}
4	10	2900	3.01×10^{-2}	8.538×10^{-7}	1.707×10^{-6}	8.538×10^{-7}
5	100	2900	3.05×10^{-1}	8.812×10^{-6}	1.762×10^{-5}	8.812×10^{-6}
6	1000	2900	3.054	8.836×10^{-5}	1.767×10^{-4}	8.836×10^{-5}

Table 4.2. Mass flow rate of propellant and non-propellant (reactor material) effluents.

5. NTR Plume Modeling

5.1 DSMC-PIC Modeling Approach

Using the results from the VNAP2 nozzle calculations, the chemistry and the material loss models described earlier and the frozen flow assumption, the species composition at the nozzle exit can be evaluated. Results are shown in Table 5.1 and are based on a radiation absorption of $\dot{Q}_r=10^5$ Wm^{-3}. Table 5.1 lists a variety of parameters at the centerline of the nozzle exit which help to characterize the DSMC simulations.

The *K*n defined with respect to the nozzle diameter D_e=2 m shows that the flow at the exit is within the continuum regime. However, as the flow expands rapidly it becomes rarefied and is therefore amenable to a particle simulation approach. This flow behavior is especially important in the nozzle lip area that is predominantly determinant of the backflow. As Table 3 indicates the difference in concentration of the neutral plume species is close to seven orders in magnitude. In addition, the small fraction of ionized component can lead to significant plasma effects. In this study we begin the development of a combined DSMC and Particle-in-Cell (PIC) code capable of addressing the complex neutral and plasma transport phenomena in the plume backflow. The

Case	1	2	3
P_c(kPa)	10	100	1000
T_c (K)	2700	2700	2700
n (m^{-3})	3.706x10^{20}	3.845x10^{21}	3.754 x10^{22}
λ(m)	8x10^{-3}	9.193x10^{-4}	9.186x10^{-5}
Kn (λ/D_e)	4.602x10^{-3}	4.596x10^{-4}	4.593x10^{-5}
H (m^{-3})	0.273	0.06	0.018
H_2 (m^{-3})	0.726	0.94	0.982
H^+ (m^{-3})	3.98x10^{-5}	3.98x10^{-6}	3.98x10^{-7}
H_2^+ (m^{-3})	7.57x10^{-7}	7.57x10^{-8}	7.57x10^{-9}
ZrC (m^{-3})	4.3810^{-7}	4.99x10^{-7}	5.12x10^{-7}
$U_{0.1}Zr_{0.9}C$ (m^{-3})	7.66x10^{-7}	8.72x10^{-7}	8.95x10^{-7}
UC (m^{-3})	1.74x10^{-7}	1.98x10^{-7}	2.03x10^{-7}

Table 5.1. NTR nozzle exit species composition at the centerline.

basic elements of the methodology and code are reviewed here. Preliminary simulation results are presented and the flow field structure, backflow and species separation issues are discussed.

5.1.1 Physical and Computational Space

A typical computational domain used in the simulations is shown in Figure 5.1. The domain extends downstream to a distance Z_{max} and at a radial distance R_{max} from the plume centerline. A surface is located at a radial distance R_e from the centerline with an axial length indicated by S. The nozzle lip extends the top surface by an axial distance L.

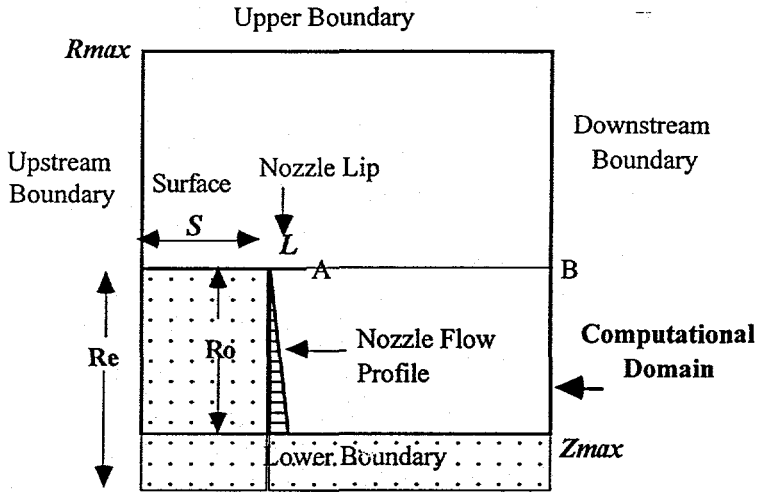

Figure 5.1. Typical computational domain used in the simulations.

The surface (S) and lip (L) are assigned as a double surface without thickness. The lower boundary can be located at a distance R_o below the surface S. In cases where the lower boundary does not coincide with the plume axis, it is approximated as a stream of temperature, density and velocity equal to those of the core flow of the NTR. This is especially useful in high density plumes where computational requirements become enormous and the particle simulations of large plume regions is computationally inefficient. The nozzle exit profile is placed at an axial distance S from the left boundary and has a radial width of R_o. This allows the species concentration, temperature, and mean axial and radial velocity to vary from cell to cell so that the exit profiles, as taken from VNAP2 or any other CFD code, can be inserted into the code. A typical flow

profile used to generate the inputs to the DSMC-PIC code is shown in Figure 5.2. This profile corresponds to Case 1 with 10 kPa and 2,700 K and the plotted variables are normalized with respect to values at the centerline. The development of the boundary layer can be seen as the thin region with a reduction in the axial component of the velocity and density, and an increase in temperature. The radial velocity component is shown to increase from the centerline until the edge of the boundary layer and then decrease.

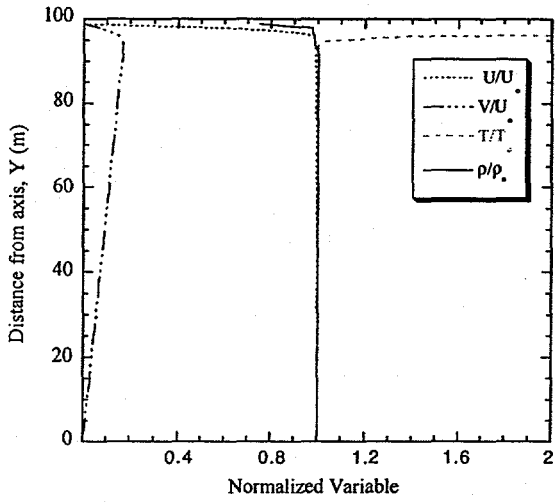

Figure 5.2. NTR nozzle exit flow profile used as input to the DSMC-PIC (Case 1: P_c=10 kPa, T_c=2,700 K). Variables are normalized to the values at the centerline.

5.1.2 Variable Particle Weight Approach

As shown in Table 5.1, the concentrations of different species critical to an NTR contamination study vary by nearly seven orders of magnitude. Clearly, a single ratio between real and computational particles (W) is impractical. Therefore, multiple Ws have to be incorporated into the code to allow for consistent selection of collision pairs, transfers of momentum and energy, and sampling of fluid properties. In addition large variation in molecular masses between the light hydrogen and the heavy reactor species affects collision rates and species separation [*Bird*, 1988, 1994; *Chung et al*, 1992, 1993]. Variable Ws are also required for the correct treatment of the ionic species, since PIC requirements for species population of cells are different from the DSMC ones. In addition to the different weights the code incorporates the grouping of species in order to account for the large mass differences as discussed by *Bird* [1994].

The NTC method developed by Bird is modified to account for the different Ws. For a gas mixture with species p and q the probability of a collision between two particles P_{pq} is

$$P_{pq} = W_q \sigma_{pq} c_{pq} \Delta t / V_C \tag{5.1}$$

where σ is the cross section, c the relative velocity and V_C is the cell volume. The number of collision pairs selected from each cell at each time step is then

$$\frac{1}{2} N_p \bar{N}_q W_q \left\{ \left(\sigma_T c_r \right)_{pq} \right\}_{\max} \frac{\Delta t}{V_C} \tag{5.2}$$

where, N_p is the number of simulated particles of species p and $\bar{N}_q$ is the average number of simulated particles of species q. The method is capable of reproducing the correct collision rates as numerical tests have demonstrated.

The code also includes energy exchange between internal and translational modes using the methodology as described by *Bird* [1994].

5.1.3 Plasma Model

The estimates of ionized component shown in Table 5.1 demonstrate the significance of plasma component of the plume. The electric fields developed in the NTR plume are expected to affect and modify the backflow as has been demonstrated in recent simulations of ion thrusters [*Roy et al.*, 1996].

The basic elements of the plasma treatment in this code are based on a hybrid PIC methodology. Electrons are treated as a fluid following a local Boltzman distribution given by

$$n_e(\mathbf{x}) = n_{eo} \exp\left(\frac{e\phi(\mathbf{x})}{kT_e} \right) \tag{5.3}$$

where $\phi(x)$ is the potential, T_e is the electron temperature and n_{eo} the electron density at a reference potential. Ions are treated as particles with prescribed distributions. A secondary grid is constructed based on the local Debye length λ_d in order to account for charge separation and therefore the development of electric fields. The charge of the ions and electrons is assigned to the PIC grid and the electric field is solved according to Poisson's equation

$$\nabla^2\phi = \frac{e}{\varepsilon_o}\left(n_e - \sum_{species} n_i\right) \tag{5.4}$$

Collisions between the charged and neutral species are currently based on the DSMC methodology and ions in the code are moved without the influence of the electric fields. Future expansions of the code will include the electric field force on the motion as well as collisions between charged-neutral and charged-charged particles. Inclusion of forces within the framework of PIC-Monte Carlo methodologies can be found in *Gatsonis et al.* [1993].

5.1.4 Molecular Parameters

The variable hard sphere (VHS) model was utilized in all computations. Table 5.2 lists the important molecular parameters at a reference temperature of 1,000 K. The diameters for ZrC, $U_{0.1}Zr_{0.9}C$ and UC are based on Xe as direct measurements are unavailable [*Chung et al*, 1992]. In Table 5.2 the exponent in the viscosity-temperate expression imply that collisions between the light species and heavy species are closer to Maxwell interactions.

Species	Viscocity Exponent	Diameter, (d_px10^{10} m)	Mass, (m_p x10^{27} kg)
H_2	0.692	2.569	3.34
H	0.8353	2.748	1.67
H_2^+	0.692	2.569	3.34
H^+	0.8353	2.748	1.67
ZrC	0.9	4.	171.1
$U_{0.1}Zr_{0.9}C$	0.9	4.	204.
UC	0.9	4.	415.

Table 5.2. Molecular parameters used in the simulations.

5.2 Results and Discussion

5.2.1 Case 1

The computational domain for Case 1 (P_c=10 kPa, T_c=2,700 K) is shown in Figure 5.1 with R_{max}=1.5 m and Z_{max}=1 m. The grid is uniform with 200 and 120 cells in the axial and radial directions respectively. The cell size is $5x10^{-3}$ m which makes it smaller than the maximum $\lambda=8x10^{-3}$ at the centerline. Three subcells are assigned per cell in each direction. The surface S extends 0.45 m from the left boundary, and the lip length is L=0.05 m. The lower boundary is placed at a distance R_o=0.1 m below the surface. Diffuse reflection with perfect accommodation is assumed and both surfaces are assigned to a temperature of 290 K. The variable weights used are shown in Table 5.3. The total number of particles at steady state is 692,485

	Particle Weight, W				
	H_2	H	H_2^+	H^+	UC,ZrC, $U_{0.1}Zr_{0.9}C$
1	10^{15}	$5x10^{14}$	10^9	$5x10^{10}$	10^9
2	10^{16}	10^{16}	10^9	$5x10^{10}$	10^{10}

Table 5.3. Particle weights (W) used in Cases 1 and 2.

Figure 5.3 shows the total number density (Top) and velocity vectors (Bottom). The flow expands rapidly and experiences large gradients in the near lip area as expected. The number density drops by almost 3 orders of magnitude before it reaches the backflow plane. The turning of the flow begins at the end of the lip and the velocity becomes almost vertical at the plane above the lip as Figure 5.3 demonstrates.

Figure 5.4 shows the magnitude of the axial (top) and radial (bottom) velocity components. The axial velocity increases downstream as the plume expands and becomes negative in the backflow region. The radial velocity shows the development of a small region extending from the lip area towards the centerline with small (less than 200 m/s) negative magnitudes. This is due to the compound effect of the diffuse reflection model and the impingement of the radial component of the nozzle flow on the lip surface. The magnitude of the radial component is small compared to the axial within the downstream region bounded by the line AB and the lower boundary of the

domain. The radial component is almost 700 m/s along the line AB as Figure 5.4 indicates and increases to almost 2,700 m/s as the flow expands towards the top boundary. These results agree qualitatively with those of *Chung et al.* [1992].

Figure 5.5 shows the translational and rotational temperatures. The decrease in the magnitude of both temperatures is associated with the expansion of the flow. The higher temperature region is associated with flow/surface interactions within the boundary layer region. The rotational temperature is shown to be higher than the translational temperature and the rotational model persists further downstream as compared with the translational mode. Both temperatures are shown to freeze as the flow expands downstream. The temperature behavior is consistent with previous results [*Bird,* 1988].

Figure 5.6 shows the number densities of the ionic species H_2^+ and H^+. The difference in the filling of the backflow can be attributed to the larger amount of monatomic hydrogen present in the flow. The simulation depicts the generation of the plasma cloud that can have significant effects in the backflow [*Roy et al.*, 1996a,b].

The reactor material ZrC and $U_{0.1}Zr_{0.9}C$ number densities are shown in Figure 5.7. Both species are confined to the downstream region of the plume. A similar behavior was observed for UC (not shown here). It is apparent that the heavier neutral species do not diffuse into the backflow region. Further studies with a more suitable grid structure are needed to determine these backflow fluxes more accurately. However, ionized reactor material could backflow in cases where electric fields develop within the plume. This has been observed for heavy Xe propellant and grid (Mo) material in ion thruster simulations [*Roy et al.*, 1996a,b]. The assessment of the plasma effects on the backflow requires the self-consistent evaluation of fields and is the subject of our continuing investigation.

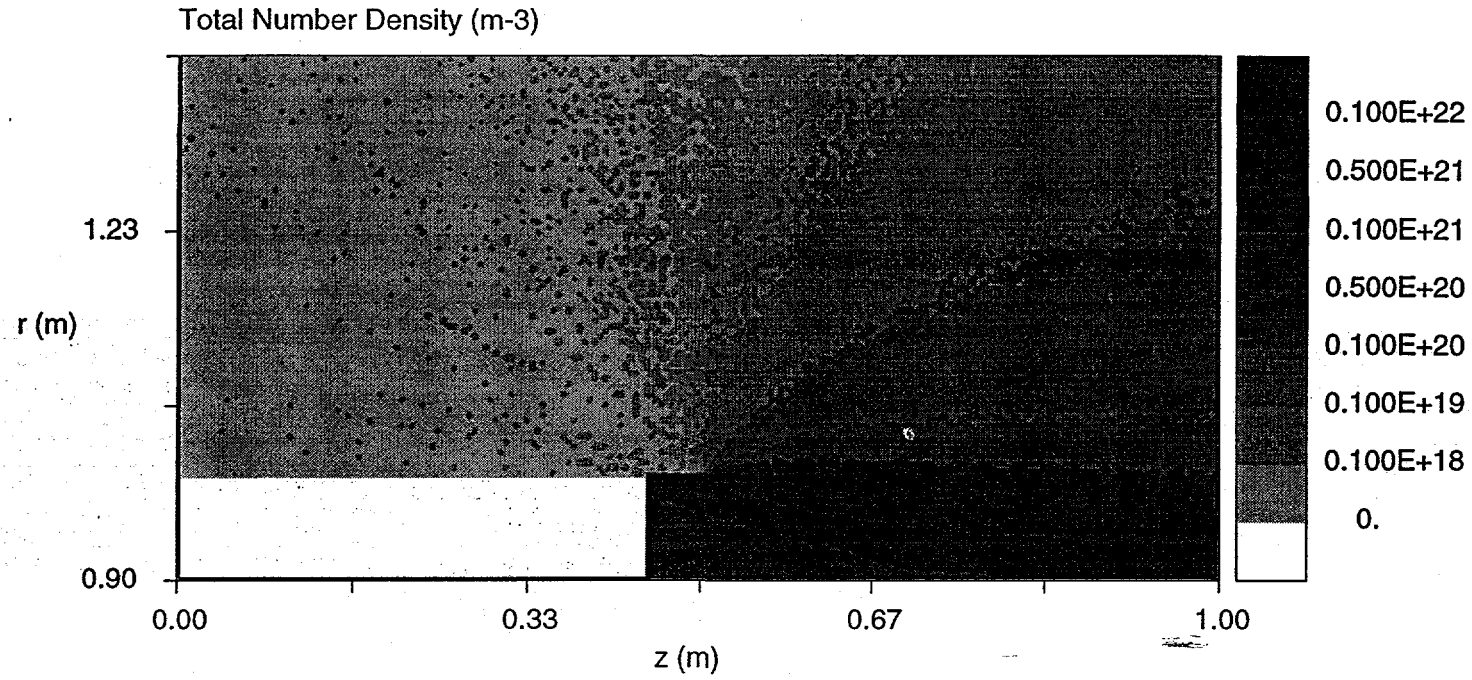

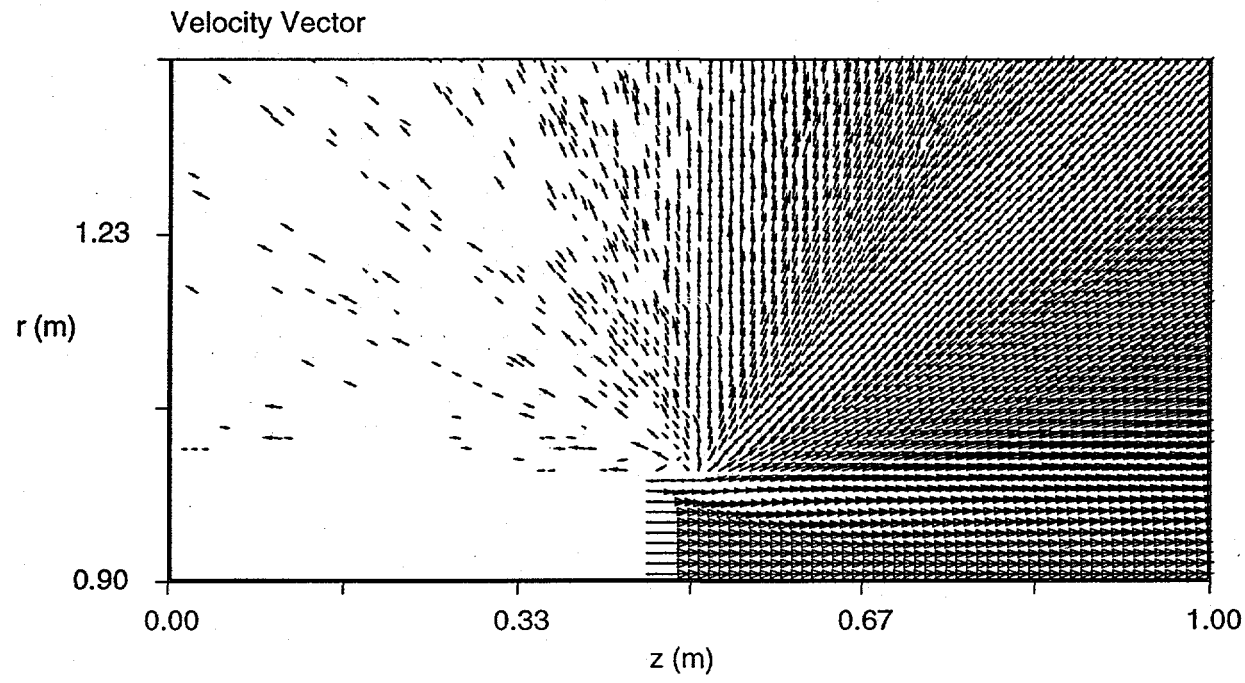

Figure 5.3 (Top) Total number density and (Bottom) Velocity vectors for Case 1 (Pc=10KPa, Tc=2700K)

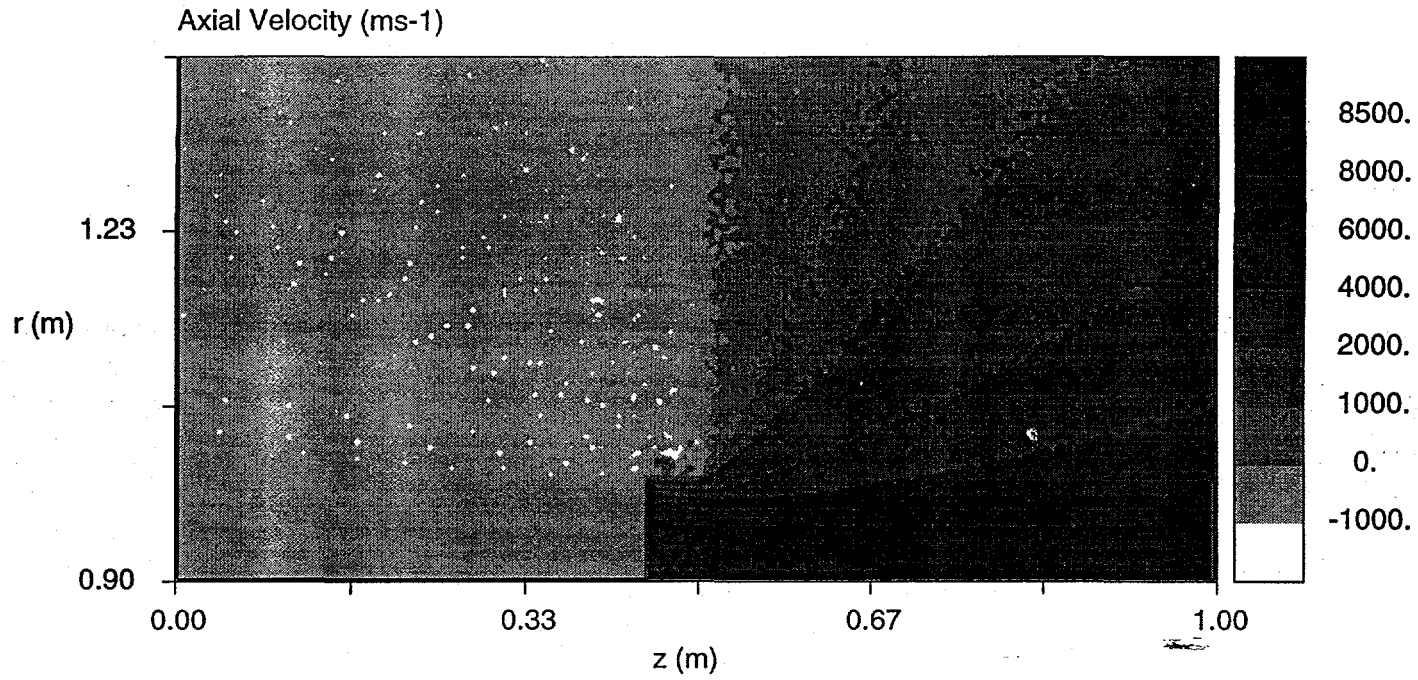

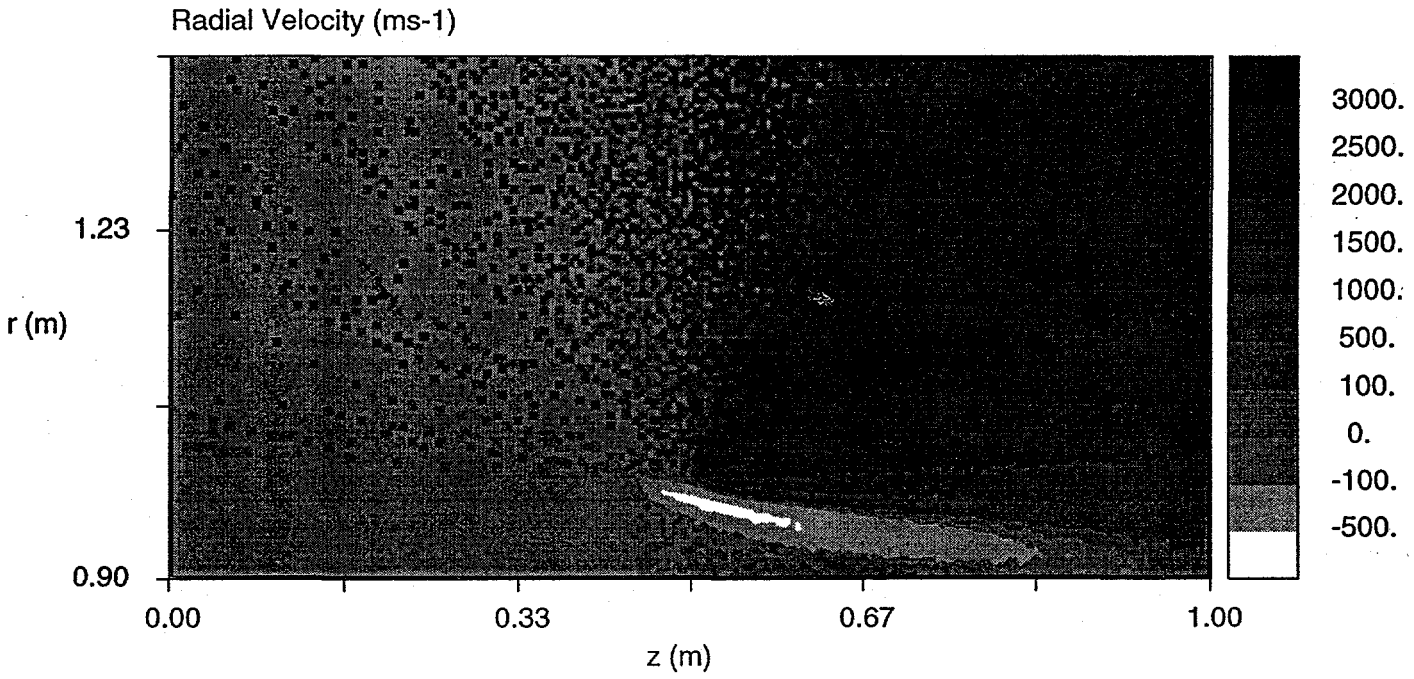

Figure 5.4 (Top) Axial velocity and (Bottom) Radial velocity for Case 1 (Pc=10KPa, Tc=2700K)

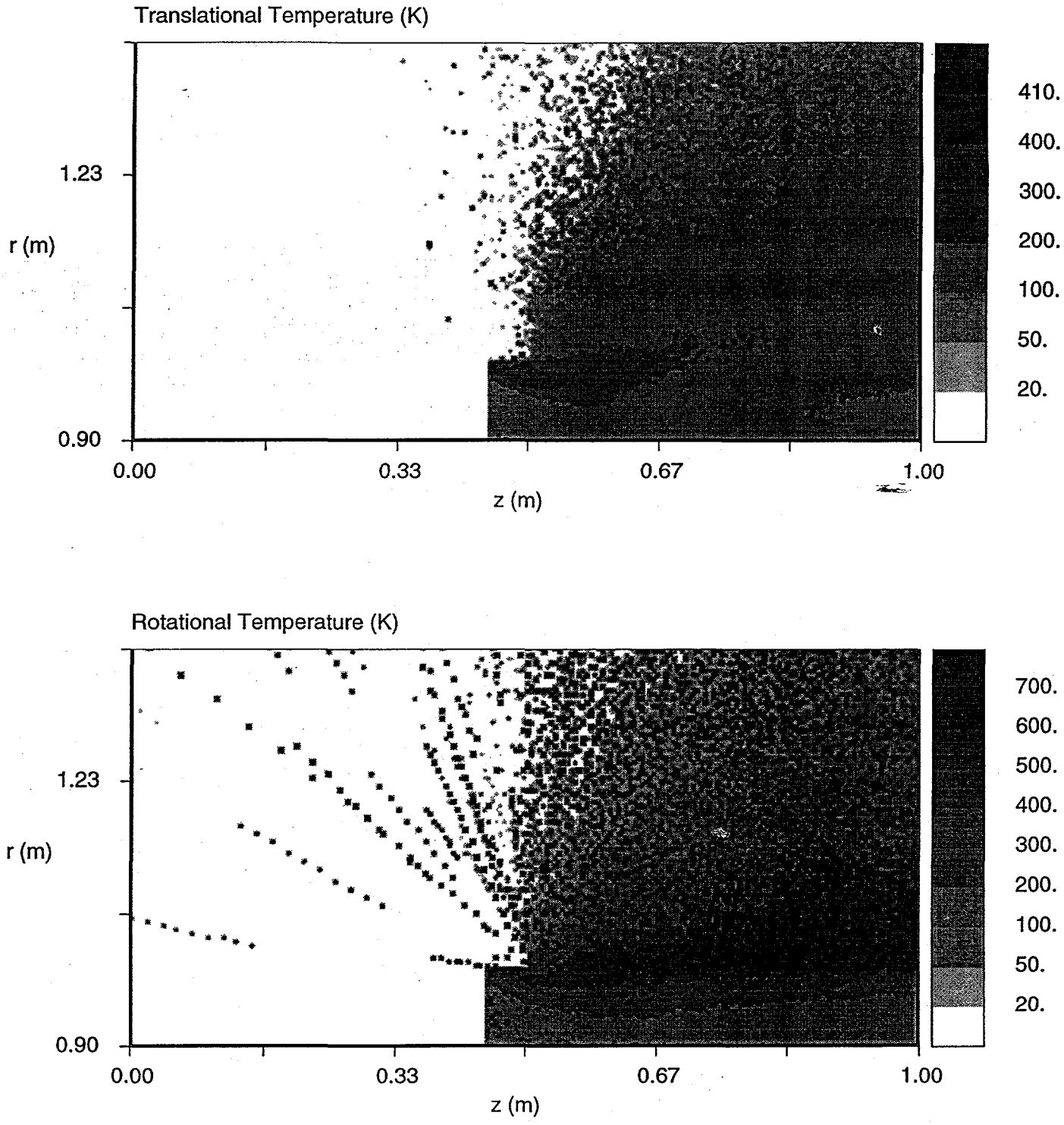

Figure 5.5 (Top) Translational temperature and (Bottom) Rotational temperature for Case 1 (Pc=10KPa, Tc=2700K)

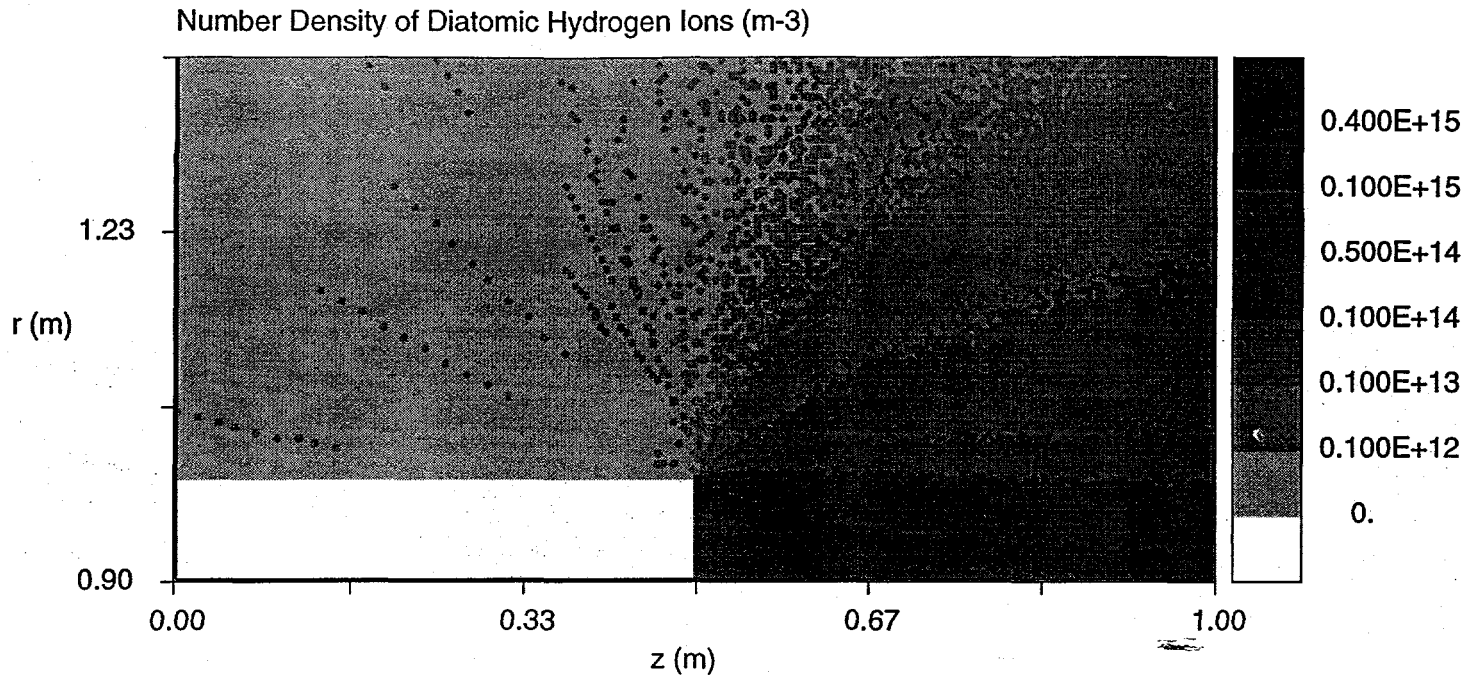

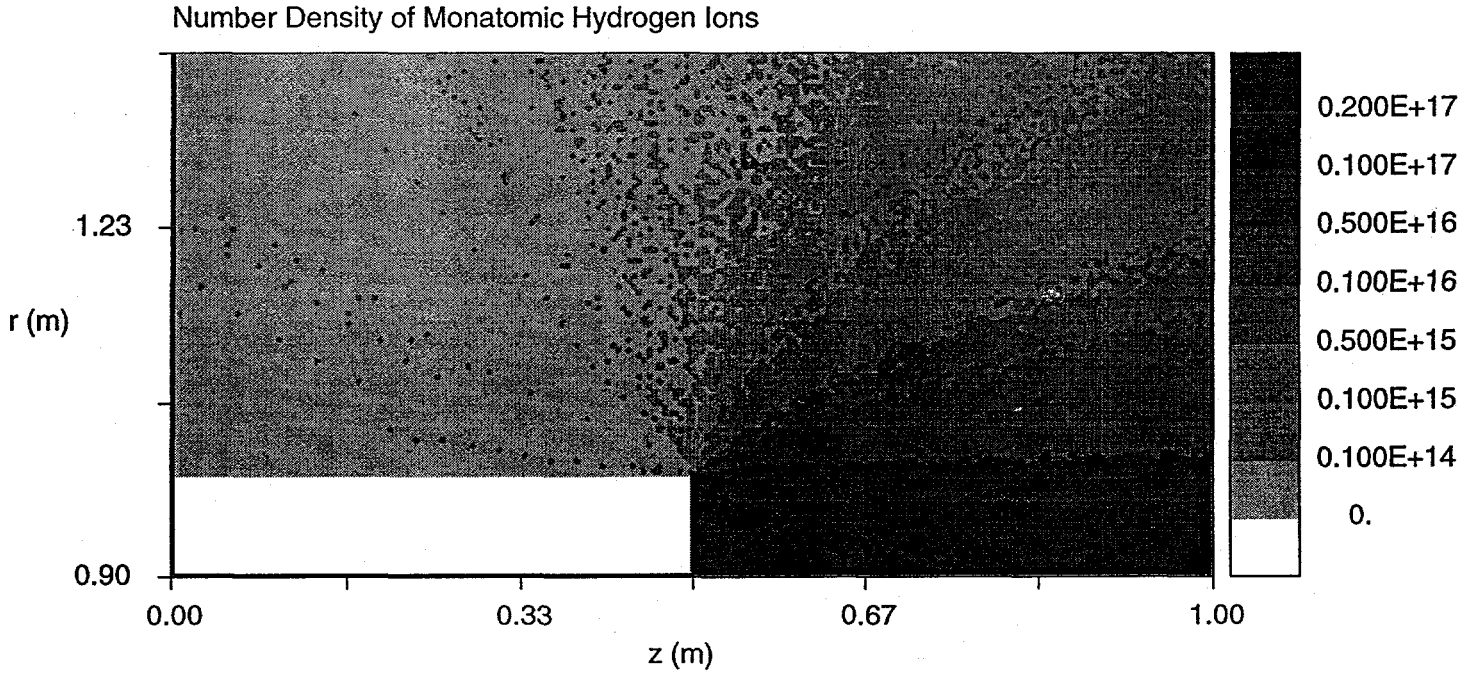

Figure 5.6 (Top) Number density of diatomic Hydrogen ions and (Bottom) Number density of monatomic Hydrogen ions for Case 1 (Pc=10KPa, Tc=2700K)

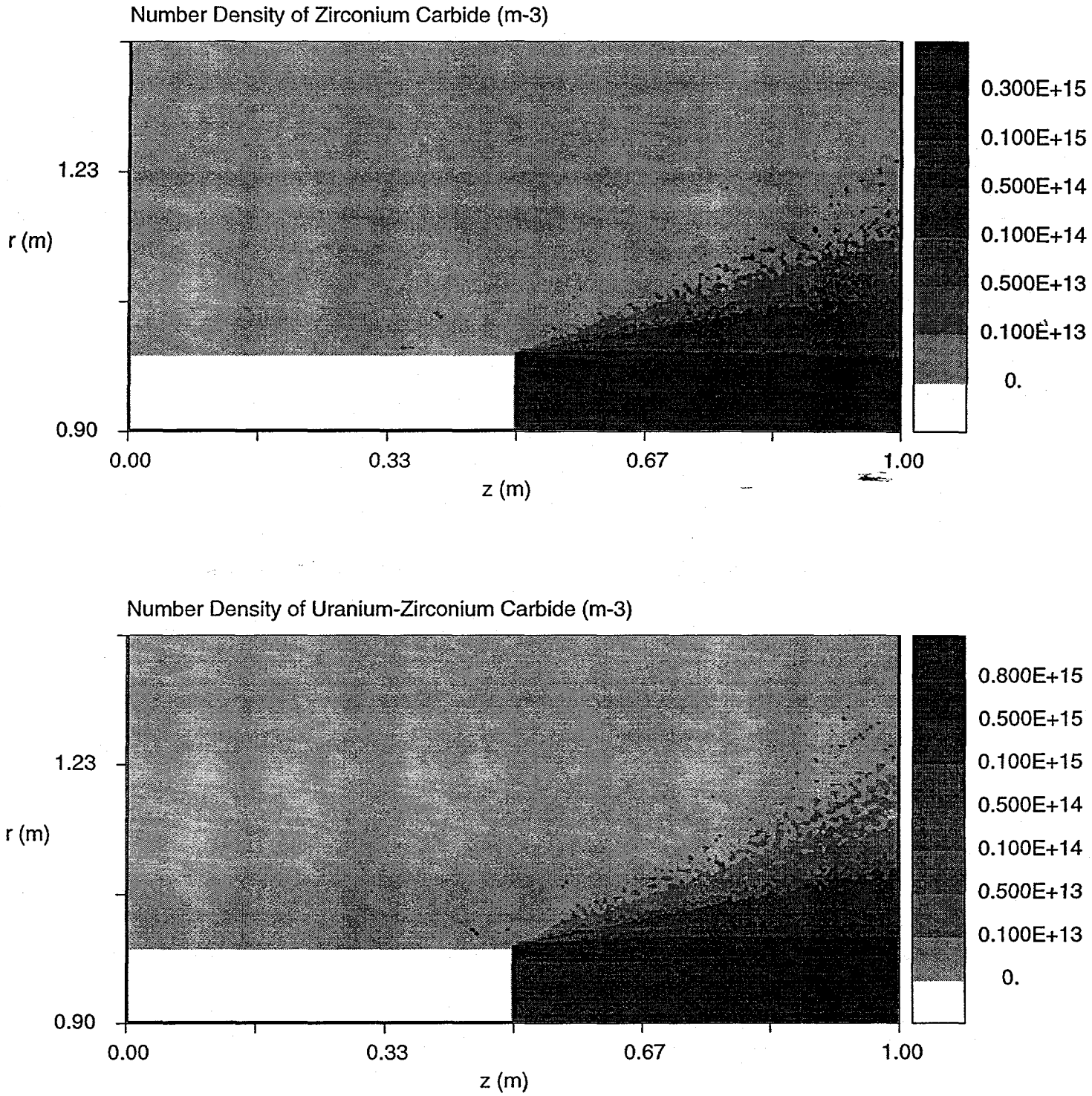

Figure 5.7 (Top) Number density of Zirconium Carbide and (Bottom) Number density of Uranium-Zirconium Carbide for Case 1 (Pc=10KPa, Tc=2700K)

A quantity often used to determine the degree of species separation in the plume defined as

$$F_i = \frac{n(i)/n(i)_o}{n(H_2)/n(H_2)_o} \tag{5.5}$$

where, n(i) is the number density of species *i* at a point, $n(i)_o$ is the number density at a reference point at the jet centerline, $n(H_2)$ is the H_2 number density and $n(H_2)_o$ refers to the same reference point [*Chung et al.*, 1992]. F_i therefore provides the local enhancement or depletion of a species and is evaluated along a horizontal line AB as shown in Figure 5.1. Species separation results for Case 1 are shown in Figure 5.8.

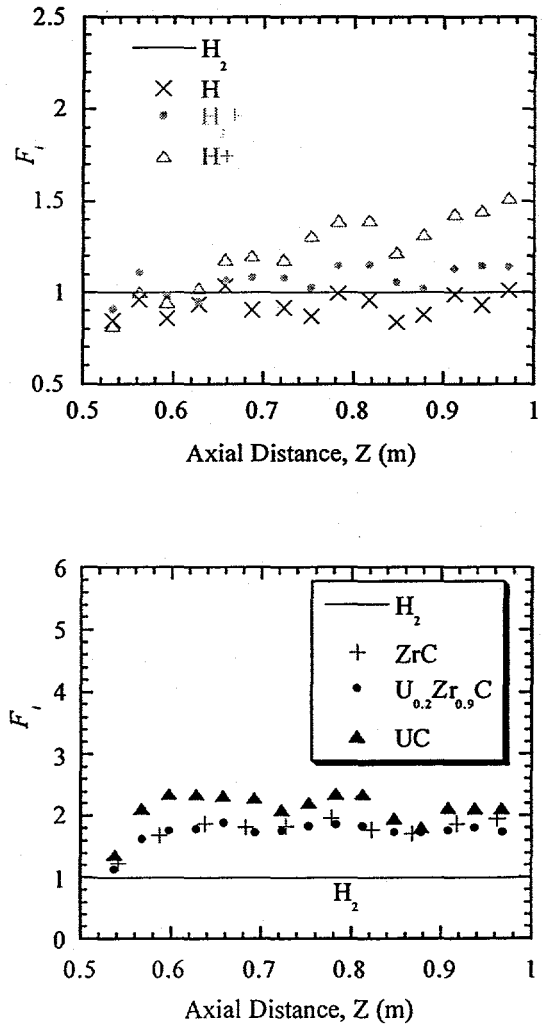

Figure 5.8. Species separation along the line AB with R=0.5 m for Case 1.

Figure 5.8 (top) shows that the light propellant species are almost constant along AB. However, the heavy species are depleted near the lip and enriched downstream the lip area as Figure 5.8 (bottom)shows. It is also shown that among the reactor material the heavier UC experiences the larger enrichment. Similar results have been obtained from *Chung et al.* [1992].

The picture of backflow can be further elaborated by calculating the mass flow rate at various backflow locations. Results are shown in Table 5.4, where Plane 1 is parallel to the thruster exit and plane 2 is at the upstream boundary of the domain (Figure 5.1). The backflow rate of H is larger than H_2 although the species fraction of H is 0.273. This higher flux is due to diffusion effects despite the very small mass ratio of the two neutral species. The rate of H^+ however is larger than H_2^+, a direct result of the two order of magnitude larger species fraction of the former.

	Plane 1	Plane 2
H_2	3.207e-7	0.0
H	4.867e-7	3.761e-8
H_2^+	5.962e-14	5.025e-14
H^+	1.701e-11	3.186e-12

Table 5.4. Propellant species mass flow rate (kg/s) through planes in the backflow region. Plane 1 is at the top of thruster exit and Plane 2 at the left boundary. Results are for Case 1.

5.2.2. Case 2

Case 2 corresponds to 100 kPa and 2,700 K chamber conditions. The exit conditions at the nozzle centerline are shown in Table 5.1. The mean free path at the centerline is approximately 8×10^{-4} m. The computational domain and grid structure used for Case 2 are identical to that of Case 1. This choice makes the cell size $\Delta c = 5 \times 10^{-3}$ m which is smaller than λ at the exit area of the plume. However, Δc becomes larger than λ at the lip and backflow area due to the significant reduction in number densities. The variable particle weights used in Case 2 are shown in Table 5.3. The cells were populated with more than 250 computational particles per cell at the near exit region. The total number of particles at steady state in the entire domain is approximately 720,000.

Figure 5.9 shows the total number density and velocity vectors. The flow exhibits qualitatively similar characteristics as Case 1 but the densities in the backflow region are much larger. The density enhancement region extending downstream the lip is also different from Case 1.

The axial and radial velocity components are shown in Figure 5.10. The region of negative radial components is smaller than Case 1. The radial velocity increases from a value of approximately 600 m/s at the horizontal line AB and to a maximum at the upper boundary of approximately 2,400 m/s. The region of maximum radial velocities is located at an angle close to 60° from the lip.

The translational and rotational temperatures are shown in Figure 5.11. Both exhibit a decrease downstream the thruster exit due to the gas expansion. The temperature freezing phenomena are depicted in Figure 5.11 as well as the effects of the boundary layer. As with Case 1, the rotational levels are higher than the translational. The region of enhanced rotational temperature downstream the lip is more confined as compared to Case 1. This is a direct result of the thinner boundary layer in Case 2 compared with that of Case 1.

Finally, the number density distributions of the ionic and reactor materials shown in Figures 5.12. and 5.13. They are qualitatively similar to those of Case 1 but with enhanced number densities as expected.

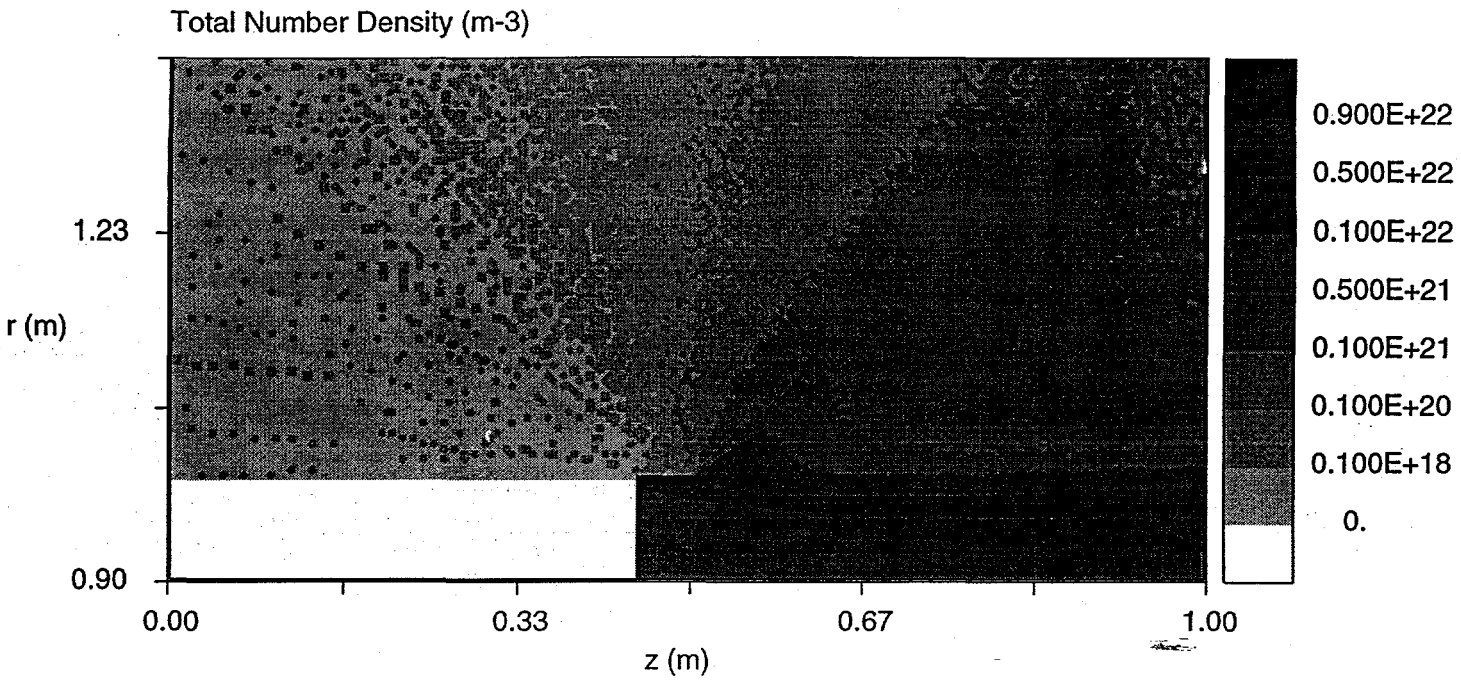

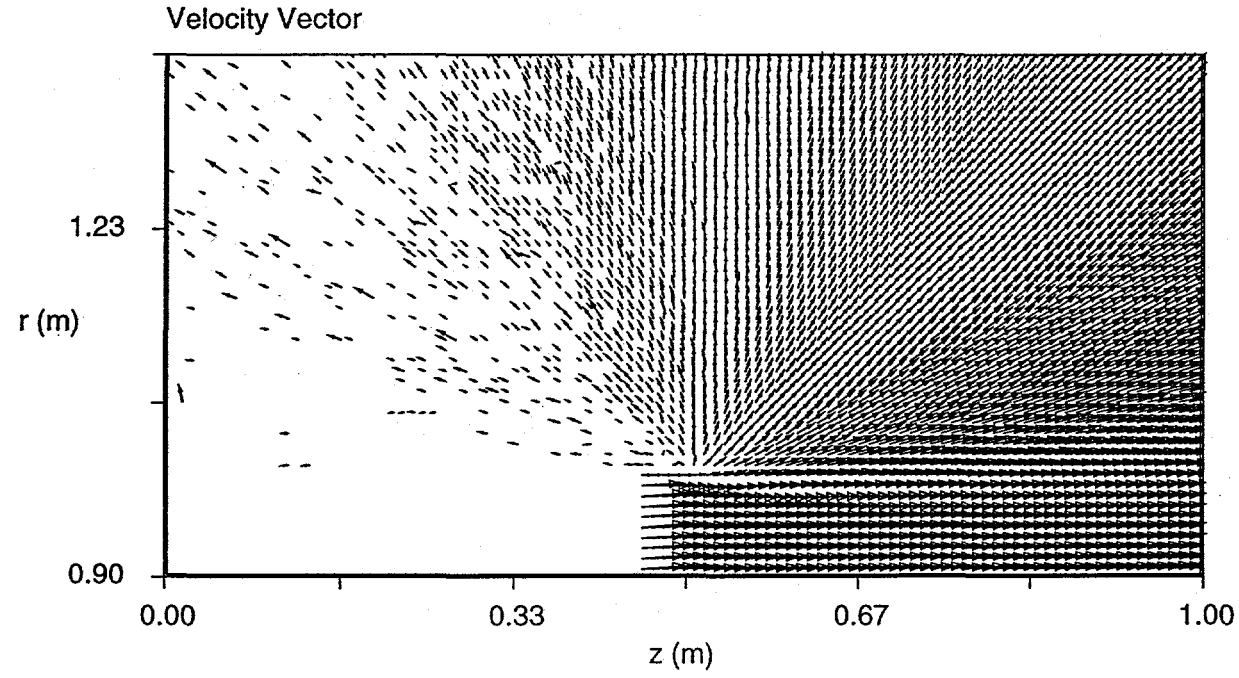

Figure 5.9 (Top) Total number density and (Bottom) Velocity vectors for Case 2 (Pc=100KPa, Tc=2700K)

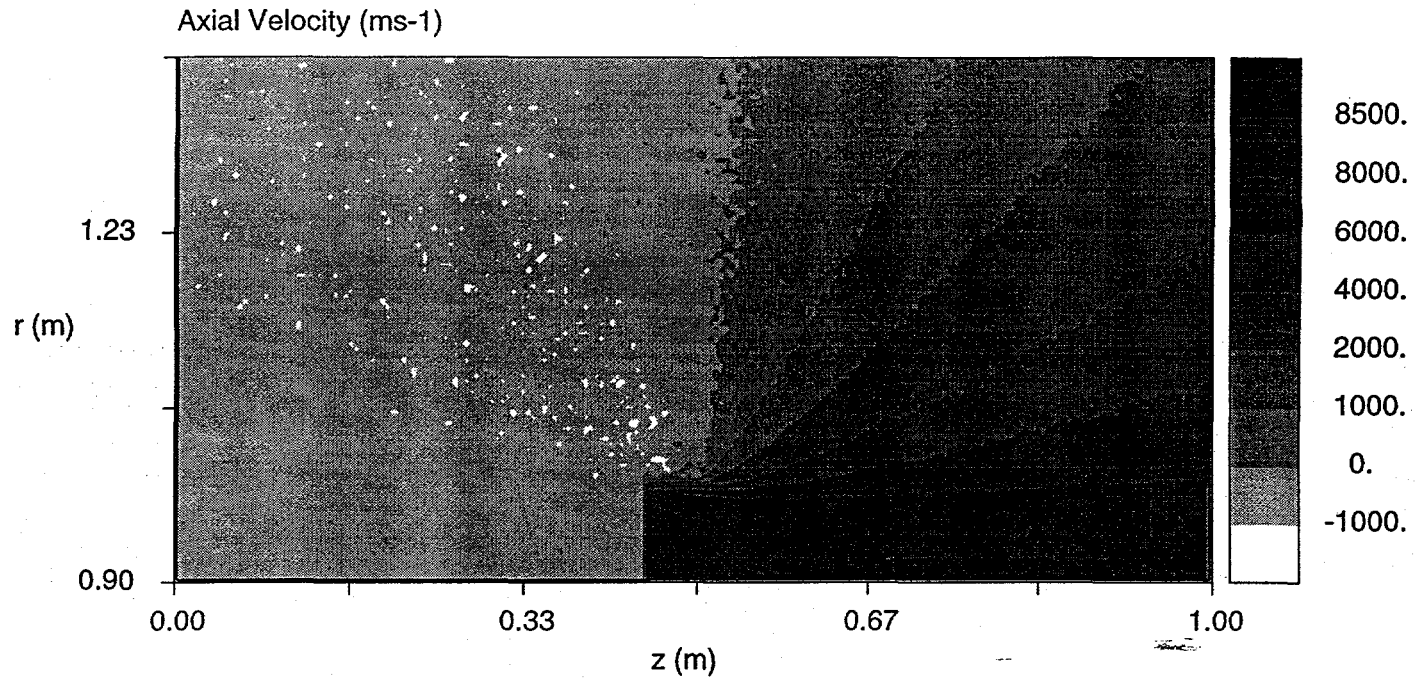

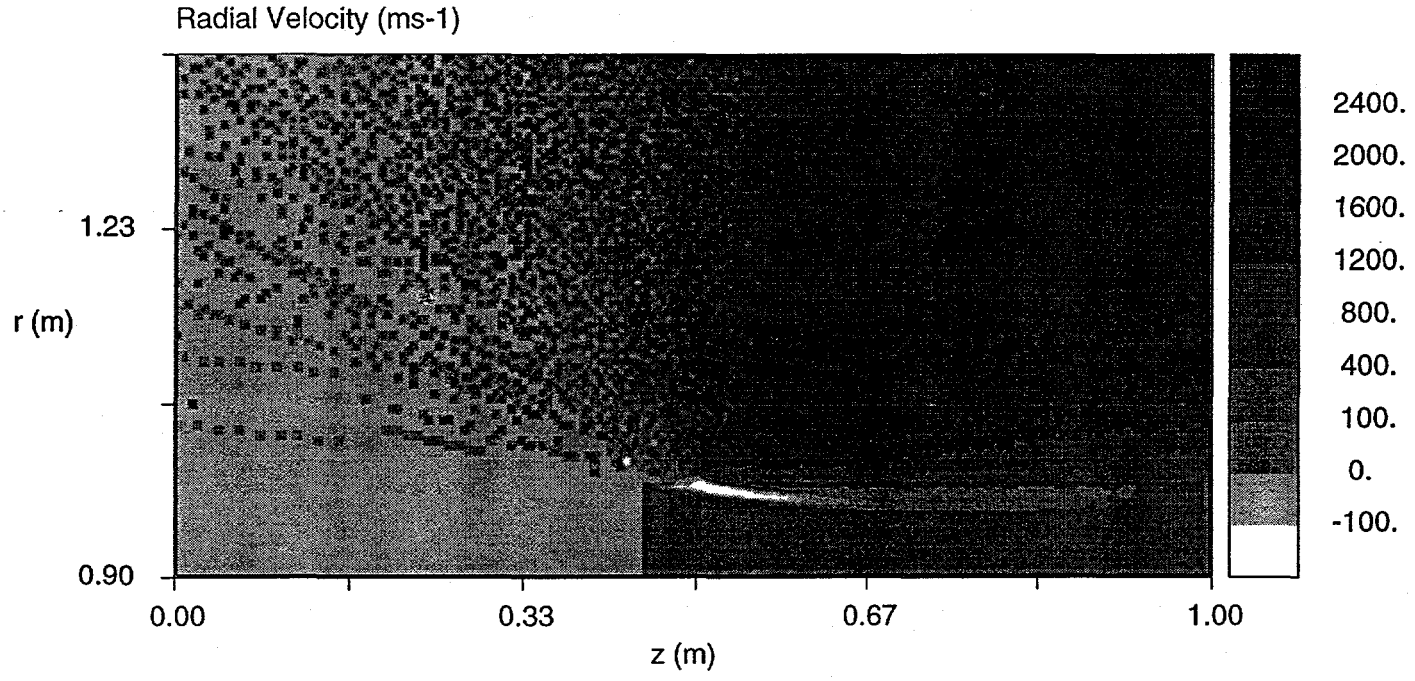

Figure 5.10 (Top) Axial velocity and (Bottom) Radial velocity for Case 2 (Pc=100KPa, Tc=2700K)

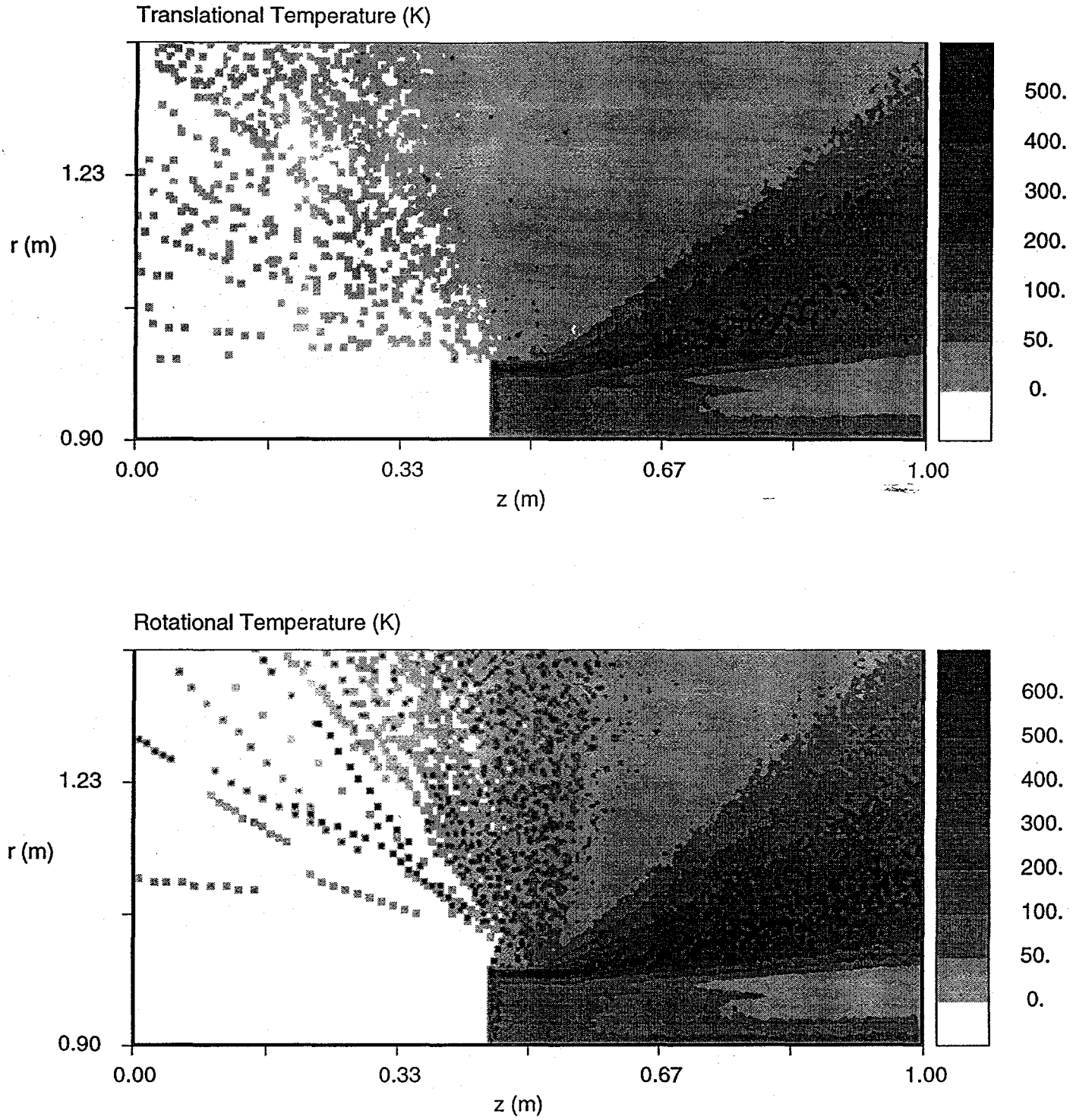

Figure 5.11 (Top) Translational temperature and (Bottom) Rotational temperature for Case 2 (Pc=100KPa, Tc=2700K)

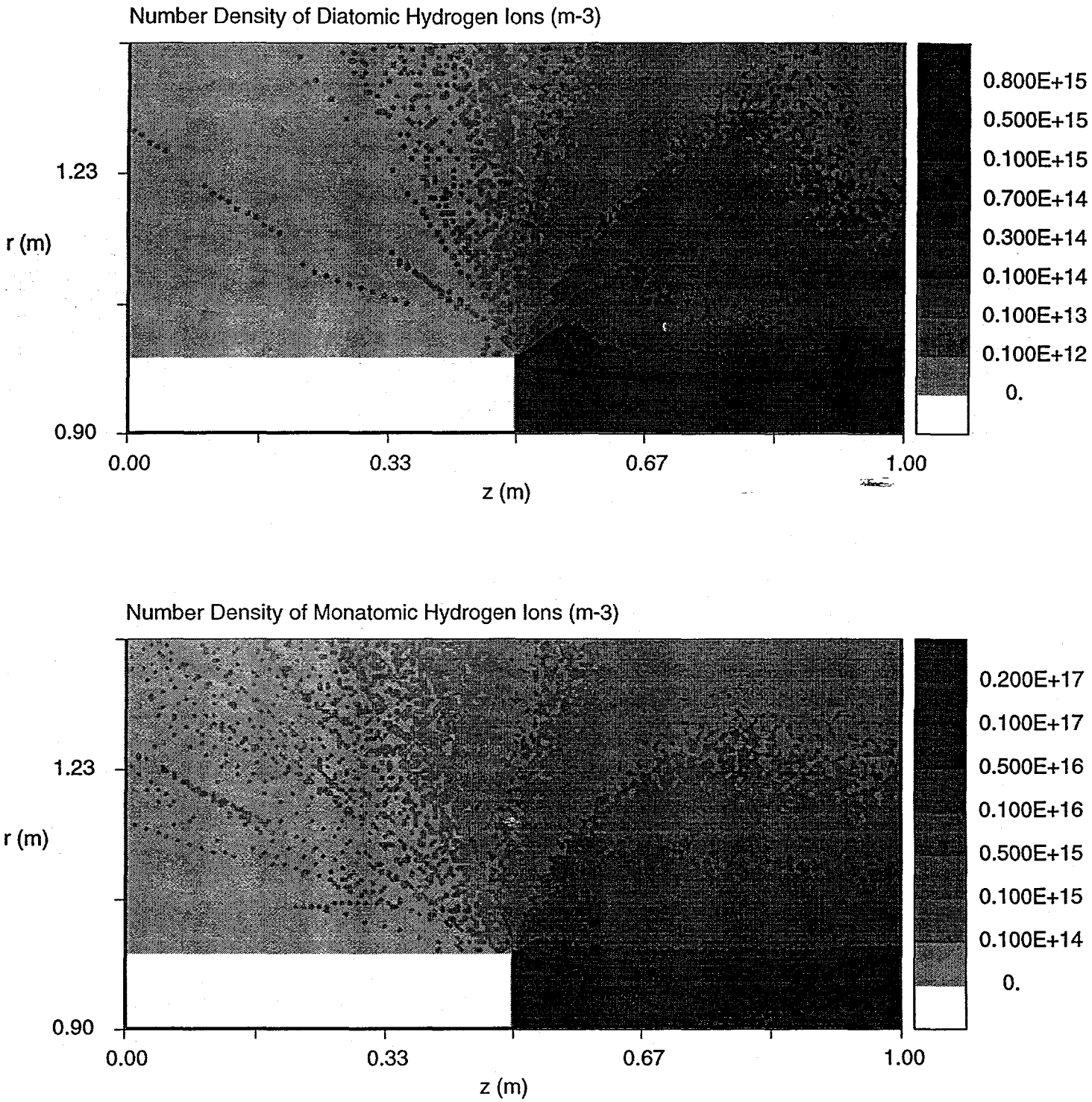

Figure 5.12 (Top) Number density of diatomic Hydrogen ions and (Bottom) Number density of monatomic Hydrogen ions for Case 2 (Pc=100KPa, Tc=2700K)

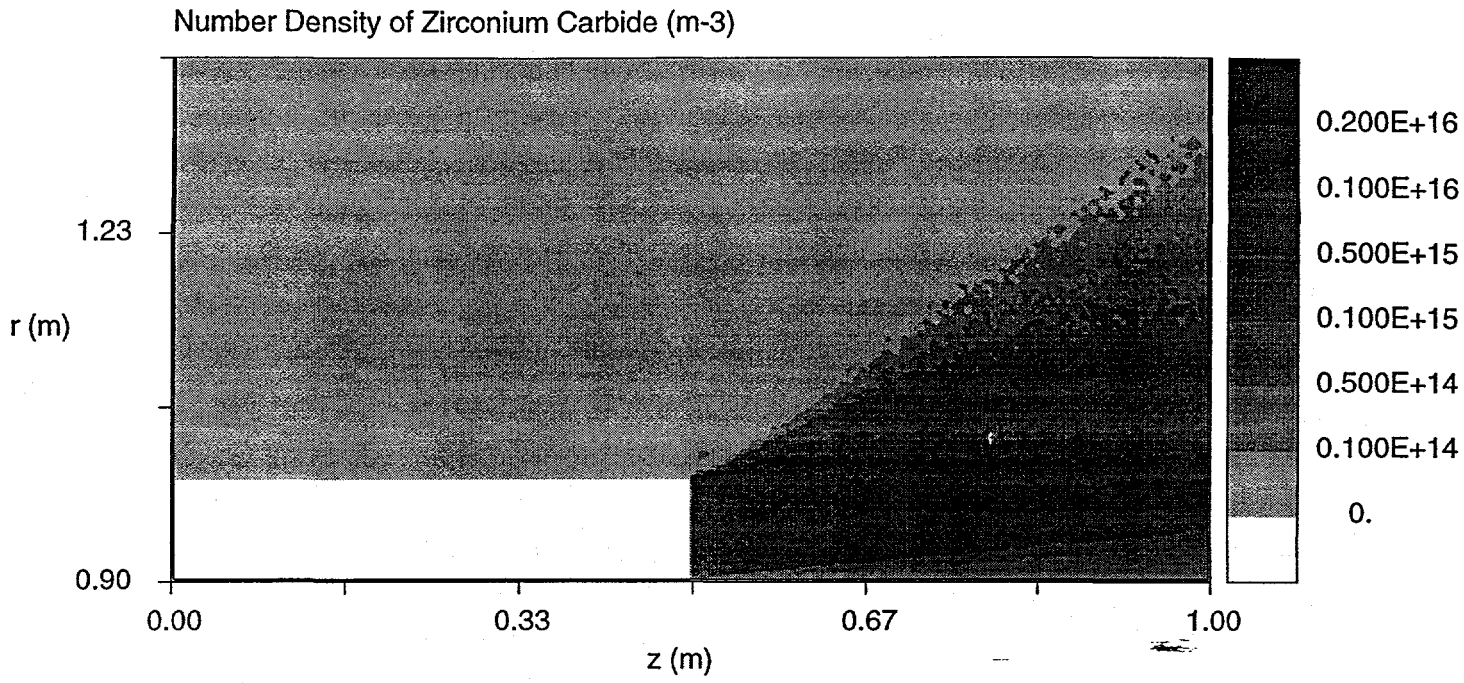

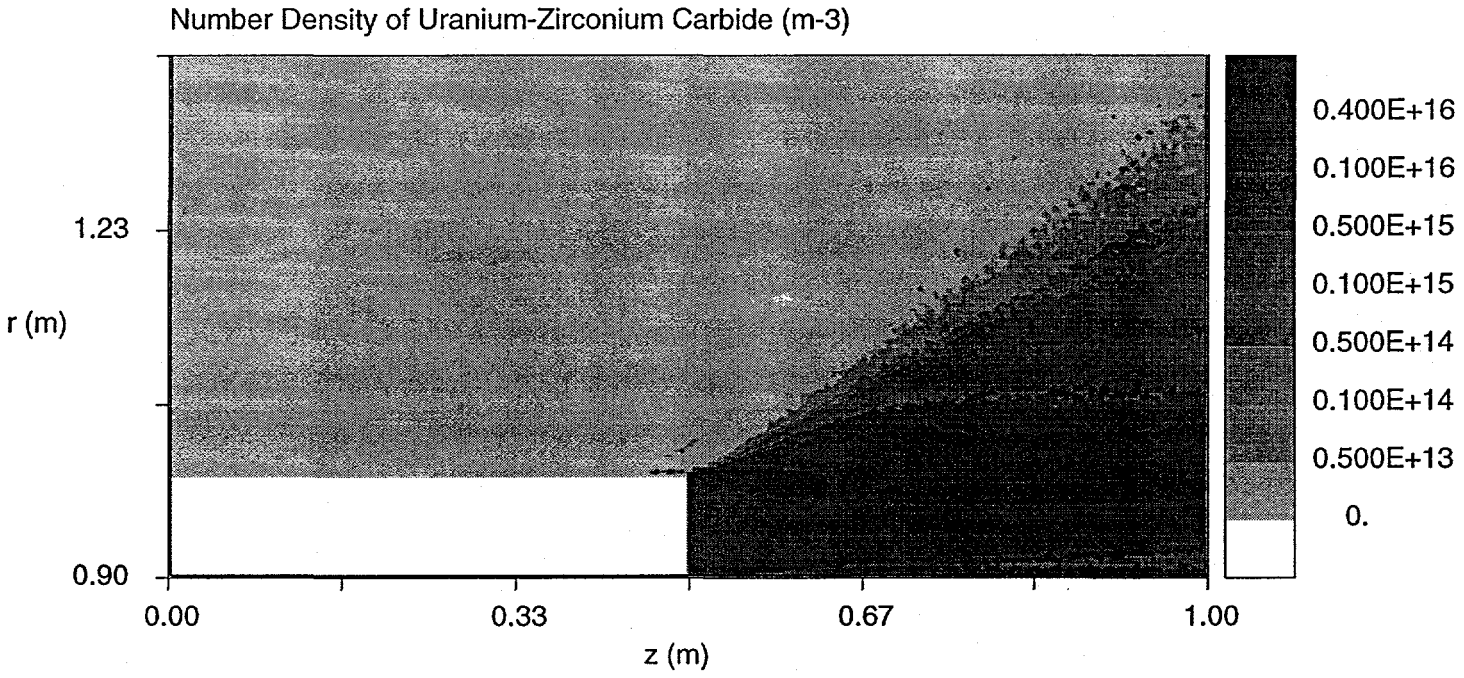

Figure 5.13 (Top) Number density of Zirconium Carbide and (Bottom) Number density of Uranium-Zirconium Carbide for Case 2 (Pc=100KPa, Tc=2700K)

The species separation along the horizontal line AB are shown in Figure 5.14 (right). The heavy species exhibit enrichment while the light species are almost constant. The magnitude of the heavy species enhancement is larger than Case 1. This is a result of the increased number of collisions in the denser plume that scatters more hydrogen particles in the backflow area.

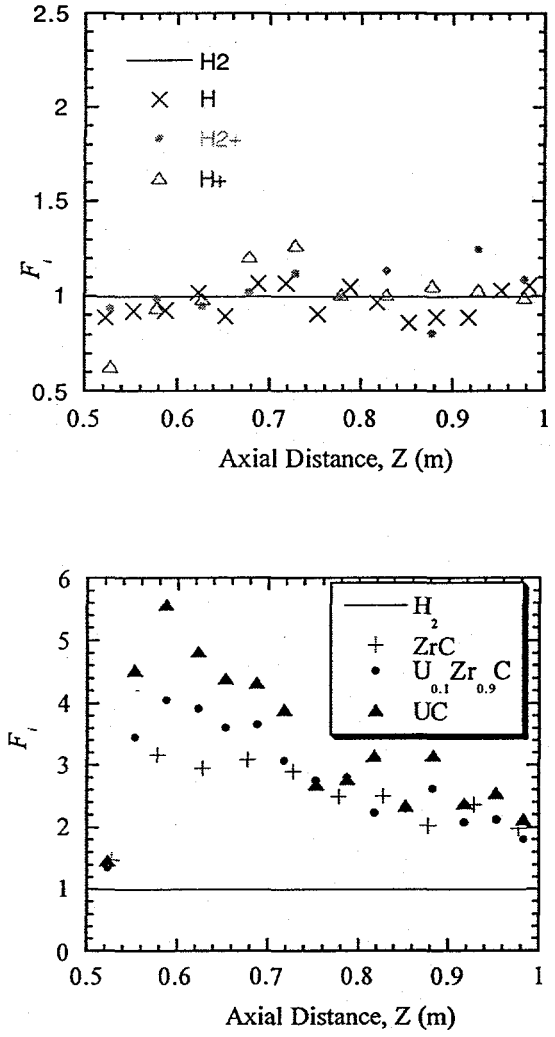

Figure 5.14. Species separation along the line AB with R=0.5 m for Case 2.

The mass flow rates at the backflow planes is shown in Table 5.5. The number fraction of H is 0.06 and the flux of H_2 becomes predominant in the backflow region. As with Case 1, the ionic

flux of H^+ is larger than the flux of H_2^+ due to the two orders of magnitude larger species fraction of the former.

	Plane 1	Plane 2
H_2	1.297e-5	5.244e-7
H	1.800e-6	1.543e-7
H_2^+	6.165e-13	0.0
H^+	1.469e-10	8.520e-12

Table 5.5. Propellant species mass flow rate (kg/s) through planes in the backflow region. Plane 1 is at the top of thruster exit and plane 2 at the upstream boundary. Results are for Case 2.

6. Conclusions and Recommendations

A study of Nuclear Thermal Rocket (NTR) effluents was presented. The NTR effluents include neutral and ionized hydrogen propellant, traces of reactor fuel material, including radioactive material and fission products. Backflow of these effluents presents a contamination risk to the spacecraft. Of particular importance is the degree of radiation induced ionization in the NTR plume. In a such a case plasma effects may become important and preferentially induce backflow of harmful radioactive species. Advanced computational methodologies and models exist for neutral and plasma plumes but not for partially ionized plumes. This study begins to asses the importance of plasma effects in an NTR plume and develop the appropriate computational methodology for accurate backflow modeling.

The NTR effluent problem was treated in this study in a unified way: the condition at the chamber were evaluated first, followed by the nozzle flow and the determination of the nozzle exit conditions. The neutral and ion propellant effluents were evaluated using a simple NTR chamber chemistry model and typical NTR operating conditions. The hydrogen ionization and dissociation was found to depend on the radiation deposition rate. The reactor material loss was also estimated using a simple model based on experimental data. The nozzle flow was calculated for a typical NTR nozzle geometry using VNAP2, an axisymmetric Navier-Stokes code. The plume composition at the nozzle exit was evaluated assuming frozen chemistry at the chamber conditions.

The Direct Simulation Monte Carlo (DSMC) and Particle-in-Cell (PIC) modifications required for the modeling of the NTR plume backflow were presented. A DSMC-PIC axisymmetric code was developed and includes general inflow boundary conditions, variable ratios between computational and real particles (particle weights), and energy exchange between translational and internal modes. A secondary grid structure is used in the code for the estimation of electric fields and ion motion. The code currently does not include the self-consistent electric fields in the ion motion.

Simulation results were presented and discussed. Plume species include neutral and ionized propellant, H_2, H, H_2^+, H^+ and reactor core materials, ZrC, $U_{0.1}Zr_{0.9}C$ and UC. Simulations correspond to chamber temperatures of 2,700 K and chamber pressures of 10 and 100 kPa. The backflow characteristics and species separation confirm previous findings. The backflow area shows to be populated mostly by light propellant species while heavy reactor species are

confined in the downstream area of the thruster exit. Of importance is the generation of a hydrogen plasma cloud. The resulting electric fields may preferentially induce backflow of the heavy charged reactor species. These issues need to be addressed in the future and require modeling improvements that are discussed below.

Recommendations

Future NTR contamination studies should incorporate improvements in the effluent evaluation as well as the DSMC-PIC methodology.

- Reactor Effluent Evaluation
  A more complete model for the reactor loss rate is needed. As shown in the present study the reactor material is important due to the contamination risk that it imposes but is also crucial in the generation of the plasma cloud.

- Chemically Reacting Nozzle Flow
  The species composition at the nozzle exit should be determined by a Navier-Stokes solver that includes chemical reactions. The radiation induced ionization and dissociation should also be included in the set of reactions.

The elements of the DSMC-PIC methodology and the associated code developed in this study should be further enhanced in order to obtain accurate backflow estimates. The following are important considerations:

- Plasma Effects
  Due to the plasma component present in the NTR plume the code should be expanded to include the self-consistent evaluation of electric fields. This will provide a more complete picture of the NTR backflow.

- Grid Generation
  The development of an efficient grid generation for the DSMC-PIC code is essential for computational efficiency and accuracy. Currently the code has a limited capability by generating an orthogonal grid structure with stretching factors in both directions.

- Surface Geometry

  Currently the code allows for flat surfaces to be modeled. The inclusion of more complex surfaces in the lip area is essential and will allow a more accurate determination of the backflow fluxes.

- Collision Algorithms

  The collision methodology for charged species-neutral collision needs improvement. In addition inclusion of charged-charged particle collisions as well as of ionization reactions is necessary.

- Parameter Range

  Although this study considered realistic parameters, a thorough investigation is needed especially in the higher end of chamber pressures.

References

[1] Bird, G. A., Molecular Gas Dynamics and the Direct Simulation of Gas Flows, Oxford University Press Inc., New York, 1994.

[2] Bird, G. A., "Thermal and Pressure Diffusion Effects in High Altitude Flows," AIAA Paper 88-2732, June, 1988.

[3] Bokor, P. C., Kirk, W. L., and Bohl, R. J., "The Behavior of Fission Products During Nuclear Rocket Reactor Tests," Proceedings of the 8th Symposium on Space Nuclear Power and Propulsion Systems, edited by M.S. El-Genk and M. D. Hoover, AIP 217, Vol. 3, American Inst. of Physics, New York, 1991, pp. 1194-1206 (CONF-910116).

[4] Borowski, S. K., Corban, R. R., and McGuire, M. L., "Nuclear Thermal Rocket/Stage Technology Options for NASA's Future Human Exploration Missions to the Moon and Mars," *Proceedings of the 11th Symposium on Space Nuclear Power and Propulsion Systems*, edited by M.S. El-Genk and M. D. Hoover, AIP 301, Vol. 1, American Inst. of Physics, New York, 1994, pp. 745-758 (CONF-940101).

[5] Boyd, I. D., Penko, P. F., and Meissner, D. L., "Numerical and Experimental Investigations of Rarefied Nozzle and Plume Flows of Nitrogen," AIAA Paper 91-1363, Jun 1991.

[6] Campbell, D. H., "DSMC Analysis of Plume-Freestream Interactions and Comparison of Plume Flowfield Predictions with Experimental Measurements," AIAA Paper 91-1362.

[7] Campbell, D. H., "Nozzle-Lip Effects on Argon Expansions Into the Plume Backflow," J. Spacecraft, Vol. 26, No. 4, 1989, pp. 285-292.

[8] Chung, C. H., De Witt, K. J., Jeng, D. R., and Penko, P. F., "DSMC Analysis of Species Separation in Rarefied Nozzle Flows," AIAA Paper 92-2859, *AIAA 27th Thermophysics Conference*, Nashville, TN, Jul, 1992

[9] Chung, C. H., Kim, S. C., Stubbs, R. M., and De Witt, K. J., "Analysis of Plume Backflow Around a Nozzle Lip in a Nuclear Rocket," AIAA Paper 93-2497, *AIAA/SAE/ASME/ASEE 29th Joint Propulsion Conference and Exhibit*, Monterey, CA, Jun 1993.

[10] Clark, J. S., Walton, J. T., and McGuire, M. L., "An Improved Heat Transfer Configuration for a Solid-Core Nuclear Thermal Rocket Engine," AIAA Paper 92-3583, *AIAA/SAE/ASME/ASEE 28th Joint Propulsion Conference and Exhibit*, Nashville, TN, Jul, 1992.

[11] Cline, M. C., "VNAP2: A Computer Program for Computation of Two-Dimensional, Time-Dependent, Compressible, Turbulent Flow," Los Alamos National Lab., Rept. LA-8872, Los Alamos, NM, Aug. 1981.

[12] Corban, R. R., "NTP System Definition and Comparison Process for SEI," *Proceedings of the 10th Symposium on Space Nuclear Power and Propulsion Systems*, edited by M.S. El-Genk and M.

D. Hoover, AIP 301, Vol. , American Inst. of Physics, New York, 1993, pp. 1713-1721 (CONF-930103).

[13] Culver, D. W., Kolganov, V., and Rochow, R. F., "Low Thrust, Deep Throttling, US/CIS Integrated NTRE," *Proceedings of the 11th Symposium on Space Nuclear Power and Propulsion Systems*, edited by M.S. El-Genk and M. D. Hoover, AIP 301, Vol. , American Inst. of Physics, New York, 1994, pp. 637-651 (CONF-940101).

[14] Davidian, K. O., and Kacynski, K. J., "Analytical Study of Nozzle Performance for Nuclear Thermal Rockets," AIAA Paper 91-3578, *AIAA/NASA/OAI Conference on Advanced SEI Technologies*, Sept. 1991, Cleveland, OH.

[15] El-Genk, M. S., Morley, N. J., and Pelaccio, D. G., "Pellet Bed Reactor Concepts for Nuclear Propulsion Applications," AIAA Paper 93-2112, *AIAA/SAE/ASME/ASEE 29th Joint Propulsion Conference and Exhibit*, Monterey, CA, Jun 1993.

[16] Gatsonis, N. A., and Hastings, D. E., "Evolution of the Plasma Environment Induced Around Spacecraft by Gas Releases: Three-Dimensional Modeling," J. of Geophysical Research, vol. 97, no. A10, pp. 1w4,989-15,005, Oct., 1992.

[17] Gatsonis, N.A., Erlandson, R.E. and Meng, C.I, "Simulation of Dusty Plasmas Near surfaces in Space", *J. Geophys. Res.-Space Physics,* 99, 1994.

[18] Hueser, J. E., Melfi, L. Tl., Bird, G. A., and Brock, F. J., "Analysis of Large Solid Propellant Rocket Engine Exhaust Plumes Using the Direct Simulation Monte Carlo Method," AIAA Paper 84-0496, *AIAA 22nd Aerospace Sciences Meeting*, Reno, NV, Jan, 1984.

[19] Johnson, R. A., Zweig, H. R., Cooper, M. H., and Wett, J., "'Fast Track' Nuclear Thermal Propulsion Concept," *Proceedings of the 10th Symposium on Space Nuclear Power and Propulsion Systems*, edited by M.S. El-Genk and M. D. Hoover, AIP 301, Vol. , American Inst. of Physics, New York, 1993, pp. 559-563 (CONF-930103).

[20] Lee, S. K., "Application of a General Fluid Mechanics Program to NTP System Modeling," *Proceedings of the 10th Symposium on Space Nuclear Power and Propulsion Systems*, edited by M.S. El-Genk and M. D. Hoover, AIP 301, Vol. , American Inst. of Physics, New York, 1993, pp. 1505-1510 (CONF-930103).

[21] Leyse, C. F., Ramsthaler, J. H., Culver, D. W., and Haloulakos, V. E., "Cost Effective Development of a Nuclear Thermal Rocket Engine (NTRE)," DOE Contract No. DE-AC07-761001570, U. S. Department of Energy, Idaho Operations Office.

[22] Mauk, B. H., Bythrow, P. F., Gatsonis, N. A., and McNutt, R. L. Jr., "Science Plan for the Nuclear Electric Propulsion Space Test Program (NEPSTP)," AIAA-93-1895.

[23] McGinnis, Muntz, E.P., Holtz, T., "A Study of the Rarefaction of the Interaction Between an Exhaust Plume and a Hypersonic External Flow", AIAA-73-199., 1973.

[24] Peery, S. D., Parsley, R. C., Anghaie, S., and Feller, G. J., "XNR2000 - - A Near Term Nuclear Thermal Rocket Concept," *Proceedings of the 10th Symposium on Space Nuclear Power and Propulsion Systems*, edited by M.S. El-Genk and M. D. Hoover, AIP 301, Vol. , American Inst. of Physics, New York, 1993, pp. 1743-1752 (CONF-930103).

[25] Pelaccio, D. G., Scheil, C., and Livingston, J., "Updated Solid-Core Nuclear Thermal Propulsion Engine Trades," AIAA Paper 91-3507, *AIAA/NASA/OAI Conference on Advanced SEI Technologies*, Sept. 1991, Cleveland, OH

[26] Pelaccio, D. G., El-Genk, M. S., and Butt, D. P., "A Review of Carbide Fuel Corrosion For Nuclear Thermal Propulsion Applications," *Proceedings of the 11th Symposium on Space Nuclear Power and Propulsion Systems*, edited by M.S. El-Genk and M. D. Hoover, AIP 301, Vol. 2, American Inst. of Physics, New York, 1994, pp. 905-918 (CONF-940101).

[27] Pelaccio, D. G., El-Genk, M. S., and Butt, D. P., "Hydrogen Corrosion Considerations of Carbide Fuels for Nuclear Thermal Propulsion Applications," JPP, Vol. 11, No. 6, Nov-Dec 1995, pg. 1338

[28] Ramasthaler,J.H, Madsen, C.F., Neumann, W.W., Schnitzler, B.C., "Low Pressure Radial Flow Nuclear Rocket Concept", NTP, July 1990.

[29] Samantha Roy, R., Hastings, D.E. and Gatsonis, N.A., "Ion-Thruster Plume Modeling for Backflow Contamination", *Journal of Spacecraft and Rockets,* V33,4,1996.

[30] Samantha Roy, R., Hastings, D.E. and Gatsonis, N.A., "Numerical Study of Spacecraft Contamination and Interactions by Ion-Thruster Effluents", *Journal of Spacecraft and Rockets,* V33,4,1996.

[31] Scheil, C. M., Pelaccio, D. G., and Petrosky, L. J., "Nuclear Engine System Simulation (NESS) Program Update," *Proceedings of the 10th Symposium on Space Nuclear Power and Propulsion Systems*, edited by M.S. El-Genk and M. D. Hoover, AIP 301, Vol. , American Inst. of Physics, New York, 1993, pp. 1523-1528 (CONF-930103).

[32] Smith, S. D., "Estimated Accuracy of Method of Characteristics Viscous Plume Solutions for On-Orbit Plume Induced Environment Predictions," AIAA Paper 91-1364.

[33] Storms, E. K., Hanson, D., Kirk, W., and Goldman, P., "Effect of Fuel Geometry on the Life Time-Temperature Performance of Advanced Nuclear Propulsion Reactors," AIAA Paper 91-3454, Sept. 1991.

[34] Stubbs, R. M., Kim, S. C., Benson, T. J., "Computational Fluid Dynamics Studies of Nuclear Rocket Performance," AIAA Paper 91-3577, *AIAA/NASA/OAI Conference on Advanced SEI Technologies*, Cleveland, OH, Sept. 1991.

[35] Stubbs, R. M., Kim, S. C., and Papp, J. L., "Analysis of Nuclear Thermal Propulsion Systems Using Computational Fluid Dynamics," *Proceedings of the 10th Symposium on Space Nuclear Power*

and Propulsion Systems, edited by M.S. El-Genk and M. D. Hoover, AIP 301, Vol. , American Inst. of Physics, New York, 1993, pp. 1569-1573 (CONF-930103).

[36] Watanabe, Y., "Radiation Enhanced Dissociation of hydrogen in Nuclear Rockets," AIAA Paper 92-3817, *AIAA/SAE/ASME/ASEE 28th Joint Propulsion Conference and Exhibit*, Nashville, TN, Jul. 1992

[37] Wetzel, K., and Solomon, W., "Effect of the Uncertainty in Hydrogen Recombination Kinetics on NTR Performance Prediction," AIAA Paper 93-2499, *AIAA/SAE/ASME/ASEE 29th Joint Propulsion Conference and Exhibit*, Jun. 1993, Monterey, CA, Jun 1993.

[38] Zweig, H. R., and Cooper, M. H., "NERVA-Derived Rocket Module for Solar System Exploration," AIAA Paper 93-2110, *AIAA/SAE/ASME/ASEE 29th Joint Propulsion Conference and Exhibit*, Monterey, CA, Jun 1993.